



High-entropy alloys: a review of mechanical properties and deformation mechanisms at cryogenic temperatures

Xuefeng Gao¹, Ruirun Chen^{1,2,*} , Tong Liu¹, Hongze Fang¹, Gang Qin¹, Yanqing Su¹, and Jingjie Guo¹

¹ National Key Laboratory for Precision Hot Processing of Metals, Harbin Institute of Technology, Harbin 150001, People's Republic of China

² School of Materials Science and Engineering, Shandong University of Science and Technology, Qingdao 266590, People's Republic of China

Received: 5 October 2021

Accepted: 27 February 2022

Published online:

21 March 2022

© The Author(s), under exclusive licence to Springer Science+Business Media, LLC, part of Springer Nature 2022

ABSTRACT

High-entropy alloys (HEAs) are multi-component alloys with a novel designed concept. These HEAs exhibit unique composition design and structural characteristics leading to excellent properties, which have attracted considerable attention in various fields. The extensively investigated HEAs exhibit excellent strength–ductility combination and excellent damage resistance at cryogenic temperature. Therefore, HEAs have potential applications in cryogenic temperature structural materials. It is important to study their deformation behavior and microstructural evolution at cryogenic temperature to provide the understanding needed for further alloy development. In this paper, the effects of different phase structure, grain size and stacking fault energy (SFE) on cryogenic temperature deformation behavior are reviewed. The research and development of tensile, compressive and fracture toughness of HEAs at cryogenic temperature are briefly reviewed. We discuss how individual deformation mechanisms can compete or operate synergistically with each other during cryogenic temperature plastic deformation, including dislocation slip, strain-induced twin formation and strain-induced phase transformation. In addition, the future trends and some problems faced by HEAs at cryogenic temperature are discussed, and prospects of HEAs are put forward.

Handling Editor: P. Nash.

Address correspondence to E-mail: ruirunchen@hit.edu.cn

<https://doi.org/10.1007/s10853-022-07066-2>

Introduction

Metal materials have a long development history and they play an important role. The pure metal materials with single structure are conducive to the characterization of material properties, but the materials lack comprehensive application properties. It is found that the properties of metal materials are greatly improved after alloying, so alloy materials have more extensive applications. The traditional alloys are based on one element and are alloyed by adding other trace elements. High-entropy alloys (HEAs) consist of at least five principal elements in an equal or near-equal atomic percentage (at.%) with no obvious difference between solute and solvent. HEAs were first independently reported in 2004 by Cantor et al. and Yeh et al. [1, 2]. The unique design concept becomes a hot research direction in the field of metal materials. HEAs have multi-component characteristics, which results in high-entropy effect, severe lattice distortion and sluggish diffusion [3, 4]. The mechanical properties of HEAs are strongly dependent on the microstructure of the alloys. HEAs with unique composition design and microstructure display exceptional mechanical performance, including high strength, ductility and toughness, especially at low temperatures, as shown in Fig. 1 [5]. The Cantor alloy exhibits exceptional fracture toughness of ~ 220 MPa·m $^{1/2}$ at 77 K, roughly independent of temperature. Other FCC alloys (austenitic stainless steels) become more brittle as the temperature decreases. HEAs are expected to be applied to aerospace materials, cryogenic pipelines and liquid nitrogen/oxygen vessels [6–11]. Refractory HEAs with high thermal stability have great potential applications in high temperature, such as aerogenerators [12–15]. Zr–Hf–Nb HEAs have excellent radiation resistance and are potential materials for the application of advanced nuclear structural materials in the future [16, 17]. The lightweight HEAs have low density, which will benefit applications of HEAs in the transportation sectors where lightness is critical [18].

The high-configurational-entropy effect may favor single solid solution phases (SS) over competing intermetallic compounds (IM) in HEAs. The solid solution matrix phase and the strengthening phase

structures are observed by adjusting the composition [8, 19–21]. At present, CoCrFeMnNi HEA with face-centered cubic (FCC) structure has been widely studied [6, 22, 23]. HEAs with FCC structure have the advantages of easy processing and excellent plasticity, but relatively low strength. Therefore, extensive research on strengthening properties has been carried out. The properties of HEAs are improved by introducing the second phase dispersion strengthening, interstitial atom strengthening, deformation strengthening and phase transformation [24–29]. Especially, the microstructure can be refined and the mechanical strength can be improved by cryogenic temperature rolling [30, 31]. HEAs exhibit excellent strength–ductility combination at cryogenic temperature deformation, which breaks the characteristics of ductile–brittle transition of traditional alloys. The cryogenic temperature is an inevitable environmental factor in the service of aviation materials. The real working environment of the aircraft is about 10,000 m, which corresponds to atmospheric temperature of 233 K. In high altitude and alpine areas, the working temperature of aircraft reaches 213 K. It is required that the manufacture materials of aeronautical components have high strength, good toughness, low thermal physical properties and good machinability at cryogenic temperature. Excellent strength–toughness combination of HEAs is observed at cryogenic temperature. These remarkable mechanical properties of HEAs make it a highly potential candidate for the wide cryogenic applications of the aerospace industry and have important theoretical value and engineering significance for structural materials applied in cryogenic temperature environments.

This review has investigated the recent development of HEAs at low temperatures. The mechanical properties and deformation mechanisms of common HEA systems are summarized at cryogenic temperature. The effects of grain size, phase structure and processing technology on cryogenic temperature properties of HEA are analyzed. In addition, the future trends and prospects of HEAs at cryogenic temperature are put forward. This review is expected to provide ideas for designing HEAs and improving the cryogenic temperature properties.

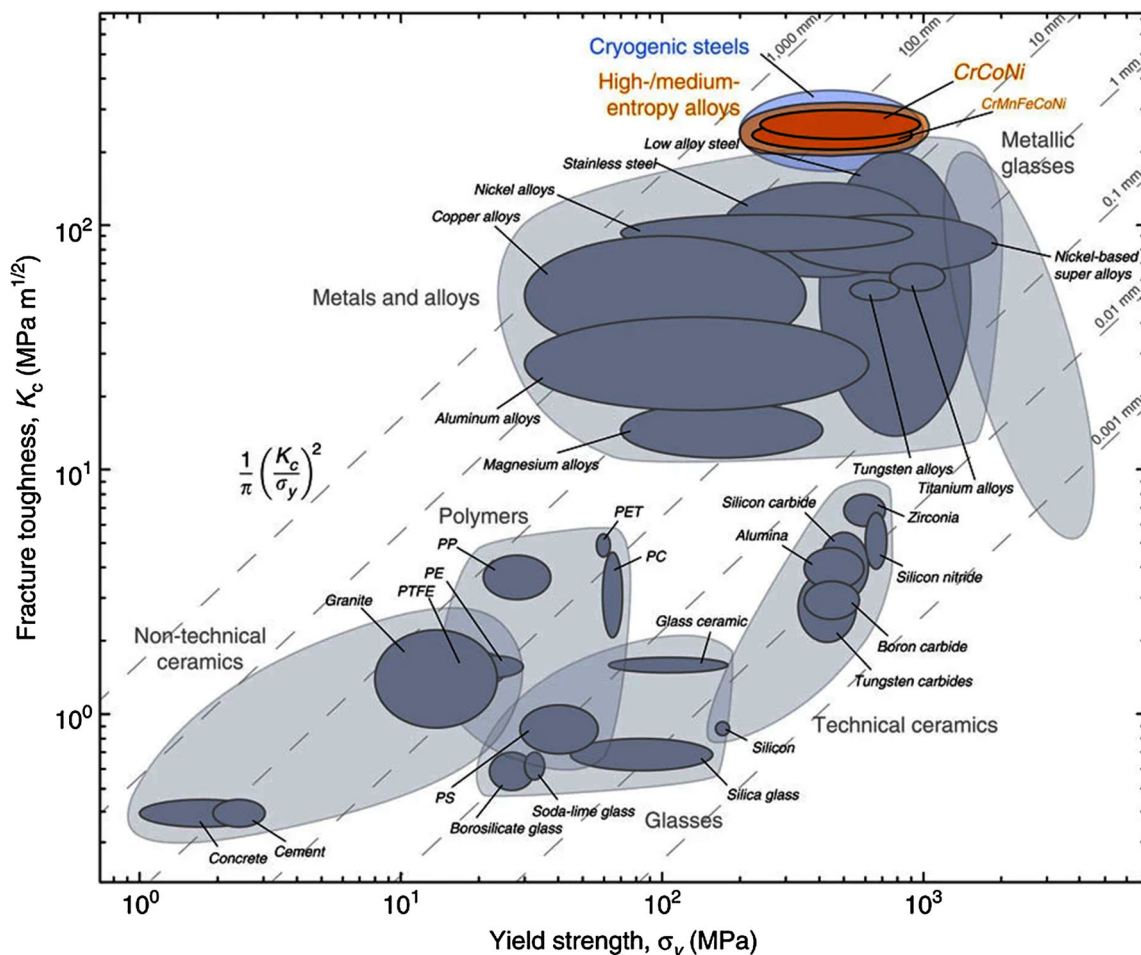


Figure 1 Ashby plot of yield strength versus fracture toughness showing CrCoNi-based, medium-entropy and HEAs at low temperature, compared with the most damage-tolerant materials

on record [5]. Reproduced from [5] with permission from Springer Nature (Author: Bernd Gludovatz).

The effects of microstructure characteristics on cryogenic temperature properties of HEAs

Effects of crystal structure on cryogenic temperature properties of HEAs

The researchers have focused on the phase structure of HEAs and have gradually developed different systems since the novel concept was first proposed. It was initially found that HEAs of different elements after equal proportion mixing do not form intermetallic or amorphous structures with complex phases. The single-phase solid solution is formed due to the high-entropy effect, and the total number of phases is well below the maximum equilibrium number allowed by the Gibbs phase rule [32–34]. With the development of HEAs, some HEAs have

multiphase structures including intermetallic compounds [35–37]. The microstructures of HEAs affect the deformation properties, especially at low temperature. The yield strength and tensile strength vs strain of different phase structures of HEAs systems is summarized at 77 K, as shown in Fig. 2 [38–50]. The single-phase FCC HEAs with high ductility present good strength, including yield strength of ~ 400 – 800 MPa and tensile strength of ~ 900 – 1350 MPa at low temperature due to deformation twinning and/or martensitic formation. The HEAs with multiphase structure exhibit high strength (yield strength: ~ 700 – 1200 MPa; tensile strength: ~ 1200 – 2200 MPa) and applicable ductility (~ 20 – 60%) by the synthesis of the FCC phase and precipitated phase at 77 K. The excellent properties of HEAs expand the application fields at low temperature.

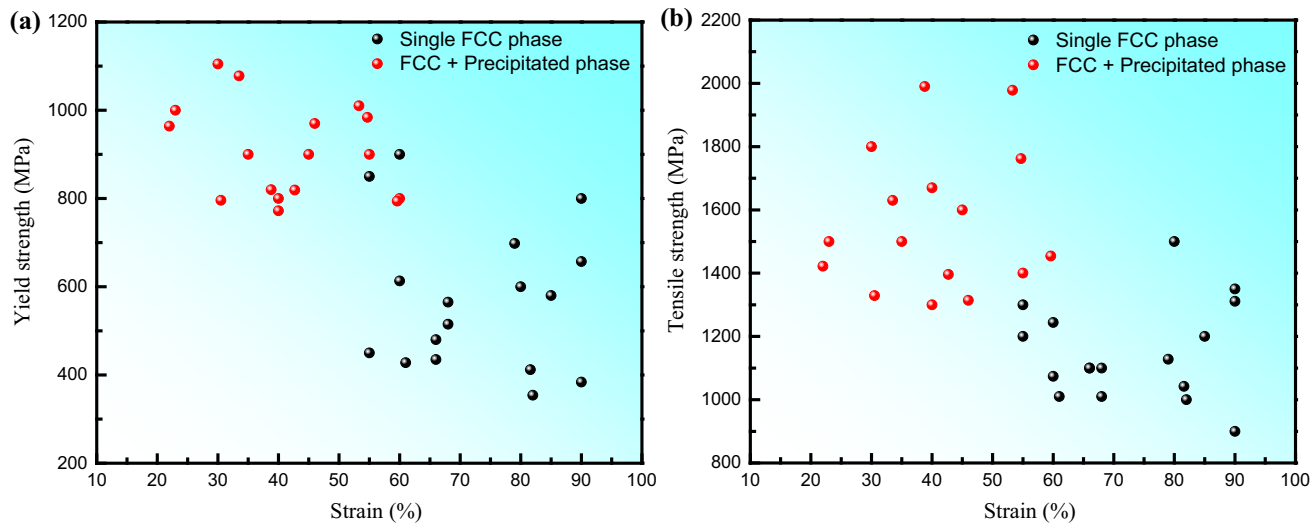


Figure 2 Tensile properties of HEAs with different phase structure at 77 K: **a** yield strength vs fracture strain; **b** tensile strength vs fracture strain.

(1) Single-phase crystal structure

Single-phase alloys generally show a ductile–brittle transition with a decrease in temperature. Austenitic stainless steels and aluminum alloys display slight reduction in ductility, but aluminum–lithium alloys have severe reduction at low temperature [51–53]. HEAs with single-phase crystal structure have been widely studied at low temperature. The yield strength, ultimate strength and elongation are simultaneously improved. In the current study, the FCC structure HEAs based on the Co, Cr, Fe, Ni, and Mn elements are the most concerned alloys. The studies show that the CoCrFeMnNi HEA (Cantor alloy) is a metastable single-phase solid solution. It precipitates into metallic BCC-Cr and intermetallic NiMn L1₀ and FeCo g phases after prolonged anneals below about 800 °C [54]. However, the solid solution state above 800 °C can be retained at room temperature. The metastable structure has a marked effect on the critical properties. The CoCrFeMnNi with single-phase FCC structure displays strongly temperature-dependent strength and ductility and modest strain-rate dependence at low temperature, due to structure instability and transformation of the HCP phase [39]. Gludovatz et al. studied CrCoNi medium-entropy alloy with single-phase FCC structure and found the improvement of strength–toughness properties at cryogenic temperature, which is attributed to a high strain hardening effect [5]. The ductility is improved

due to the postponed occurrence of necking, and the ductile micro-void coalescence is observed in the FCC structure HEAs. The SFE of FCC-based HEAs decreases with the decrease in temperatures, which induces the transformation of deformation mechanism from conventional dislocation glide to deformation twins and ε-martensite phase formation. Twinning-induced plasticity (TWIP) and phase transform-induced plasticity (TRIP) mechanisms are activated at low temperature.

Single-phase BCC HEAs have high strength, but limited plasticity at room/high temperature [55]. The cryogenic temperature properties of BCC phase structure HEAs are closely related to their constituent elements. The plasticity of AlCoCrFeNi HEA changes gradually between 298 and 77 K, which does not correspond to a brittle transition at low temperature [56]. The yield strength and fracture strength increase, and the fracture strain slightly decreases when the temperature decreases from 298 to 77 K. With the decrease in temperature, the fracture mode changes from intergranular fracture to transgranular fracture. The refractory HEAs with single BCC phase display almost negligible strain hardening ability. The yield strength of HfNbTaTiZr is 984 MPa and 1838 MPa, but the ductility is 4 and 2% at 300 and 77 K, respectively [57]. The refractory HEAs have low plasticity at room temperature and good resistance softening ability at high temperature, but the properties at low temperature are rarely studied.

(2) Multiphase crystal structure

With the development of HEAs, a large number of HEA systems based on Cantor alloy have been explored by alloying elements or adjusting the proportion of elements to further improve the properties. The structure of HEAs has gradually developed from single-phase alloys to multiphase alloys. As shown in Fig. 2, it is found that the dual-phase alloy has better comprehensive properties at low temperature. The phase structure has a great influence on the properties and deformation behavior at low temperature. A variety of strengthening mechanisms can be introduced to improve the properties, including solid solution strengthening [58], grain refinement [59], and precipitation strengthening [60–62]. AlCoCrFeNi_{2.1} eutectic high-entropy alloy (EHEA) with typical as-cast lamella morphology was engineered with an ultrafine-grained duplex microstructure by tailored thermo-mechanical processing to achieve the desired property combinations [63]. The hierarchically structural heterogeneity includes two types: NiAl-rich lamellae B2 grains (the small and scarce P1 (intragranular B2 grains) of size 50–180 nm, and the large and primary P2 (intergranular B2 grains) with an average size of ~ 350 nm) and FeCr-rich lamellae FCC grains after rolling and annealing, are shown in Fig. 3 (c–e). The tensile strength of AlCoCrFeNi_{2.1} EHEA increases obviously due to a two-hierarchical constraint effect and a self-generated micro-crack-arresting mechanism at 77 K, which provides a pathway for strengthening eutectic alloys at low temperatures [63, 64]. Multiphase structured HEAs can significantly improve the strength without seriously damaging plasticity at low temperature and such HEAs are expected to become potential materials for applications in cryogenic environments. The precipitation strengthening and nano-twins result in the increasing of strength and work hardening. The microstructure of Al_{0.5}CoCrFeMnNi HEA at cryogenic temperature is shown in Fig. 4 [65]. The geometrical necessary dislocation (GND) density of the FCC and BCC phases increases in parallel at room temperature (RT), but the GND density of FCC exhibits more active evolution and higher than that of the BCC phase at 77 K. The tensile properties improvement is attributed to the soft FCC matrix and hard BCC phase with severe strain partitioning effect with the decrease in temperature. The brittle σ-phase in HEAs results in the strength enhancement, but

significant ductility reduction at room temperature. Jo et al. designed a non-equiautomic VCrFeNi HEA to exploit the strengthening effects of σ-phase to improve cryogenic temperature properties [66]. The content of σ phase is adjusted by annealing treatment in Fig. 5. FCC grains with sizes of 1.5 μm or smaller are marked by a green color in Fig. 5(b-d) and most of the green-colored grains are surrounded by σ-phase particles. The σ phase precipitation at the grain boundary decreases grain size and effectively improves both strength and strain hardening at low temperature, which are enabled by nano-sized dislocation substructures.

Effects of grain size on cryogenic temperature properties of HEAs

At present, the grain refinement leads to the strengthening effect in HEAs due to the increase in grain boundaries. The grain size and mechanical properties of HEAs are adjusted by heat treatment and large deformation [67–69], such as rolling deformation at low temperature [70, 71]. Sathiaraj et al. investigated the effect of cryo-rolling (90%) on the evolution of microstructure during annealing in CoCrFeMnNi HEA [31]. As shown in Fig. 6, it can be observed that lamellar deformed bands extended parallel to the roll direction (RD) after rolling deformation. The finer fragmented structure forms and the grains become smaller in the lamellar boundary and shear band. After cryo-rolling, the deformation is more significant and has evidently produced a more fragmented and finer microstructure. There are many connected micro-shear bands, which may be attributed to the formation of nano-twins during deformation.

Stepanov et al. studied the microstructure evolution in CoCrFeNiMn during rolling to a thickness strain of 15%, 40% and 80% at 77 K [72]. As shown in Fig. 7, the grains are obviously elongated along the rolling direction at low temperature. At ε = 15%, the twinning in the sample after cryo-rolling is more significant. At ε = 40%, there are many intersecting micro-shear bands at 77 K, which lead to the microstructure fragmentation. The fragments size is about 2 ~ 12 μm. At ε = 80%, the more lamellar structures are formed along the deformation direction of the metal at 77 K and the fragment size is 0.3 ~ 1 μm. The grain size decreases with the

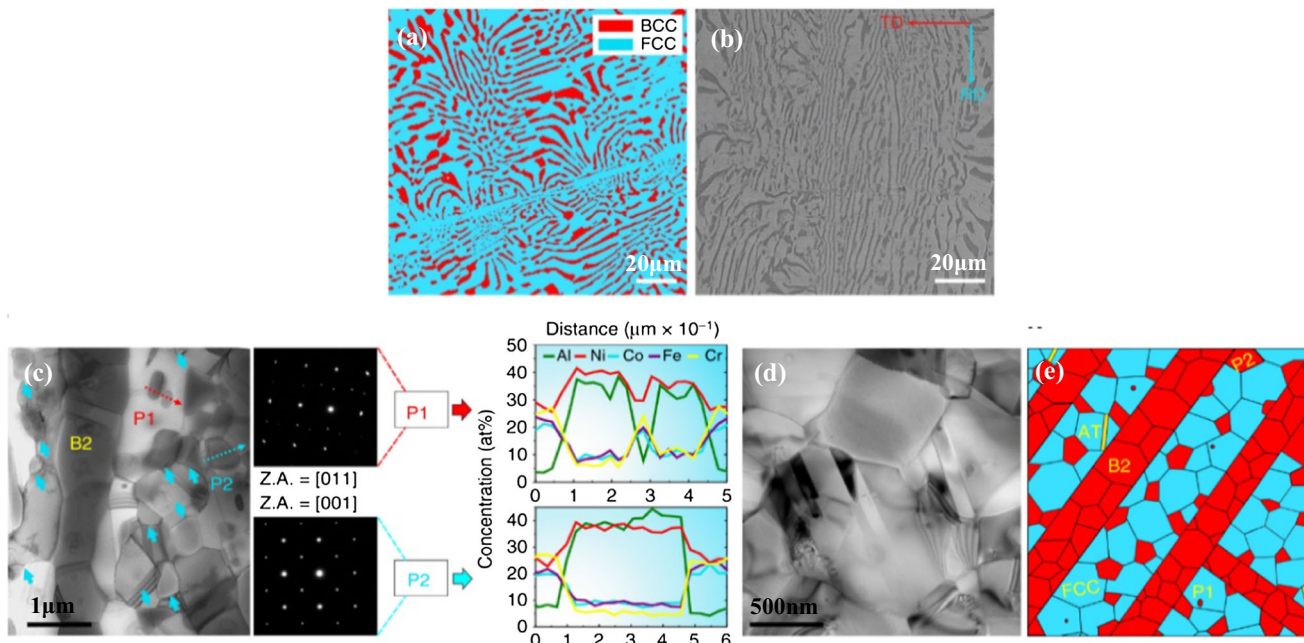


Figure 3 Microstructure of the AlCoCrFeNi_{2.1} EHEA: **a** and **b** electron-backscatter-diffraction (EBSD) phase image and scanning-electron-microscope (SEM) image of the as-cast EHEA, respectively; **c** TEM image of annealing precipitated phase distribution (P2 (the intergranular B2 phase, marked by blue arrows) and P1 (the intragranular B2 phase, marked by red arrow))

and the corresponding selected-area diffraction patterns (SADPs) and energy dispersive spectroscopy (EDS) composition profiles; **d** TEM image of annealing twins; **e** schematic sketch of annealing structure (AT: annealing twin) [63]. Reproduced from [63] with permission from Springer Nature (Author: Peijian Shi).

Figure 4 Microstructure of Al_{0.5}CoCrFeMnNi HEA: **a** XRD pattern; **b** EBSD phase map; **c** the average GND density of dual phases at RT; **d** the average GND density of dual phases at 77 K [65]. Reproduced from [65] with permission from Elsevier.

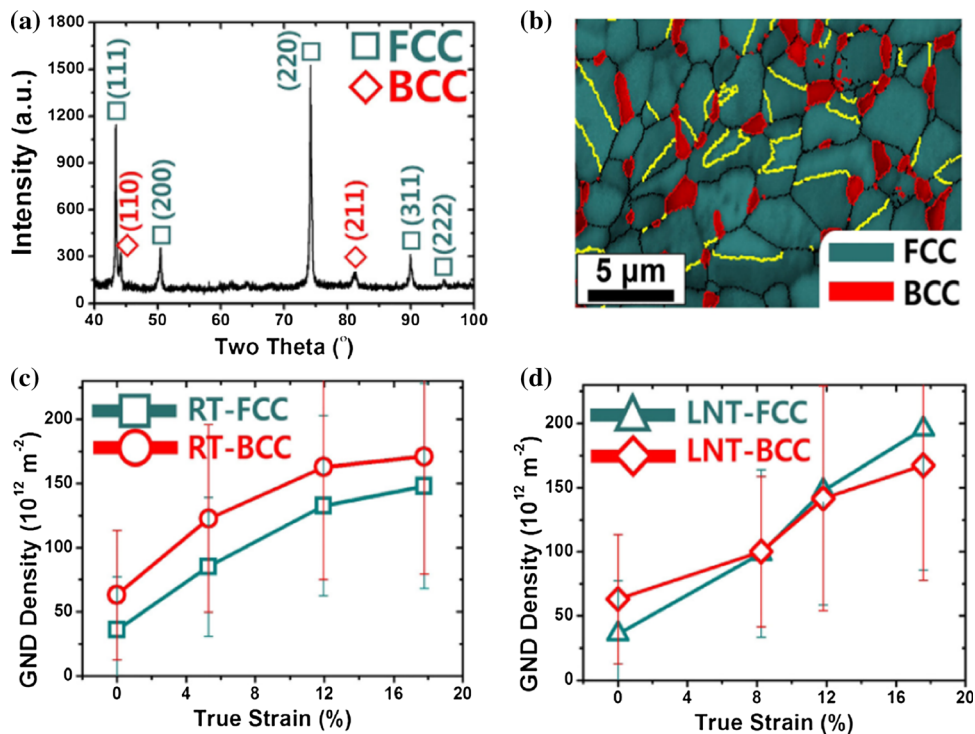


Figure 5 EBSD image quality maps of annealed $V_{20}Cr_{15}Fe_{20}Ni_{45}$ HEA at different temperature: **a** 1000 °C/10 min; **b** 950 °C/10 min; **c** 900 °C/10 min; **d** 800 °C/1 h (the specimens annealed at 1000, 950, 900 and 800 °C are referred to as 1000A, 950A, 900A and 800A, respectively) [66]. Reproduced from [66] with permission from Elsevier.

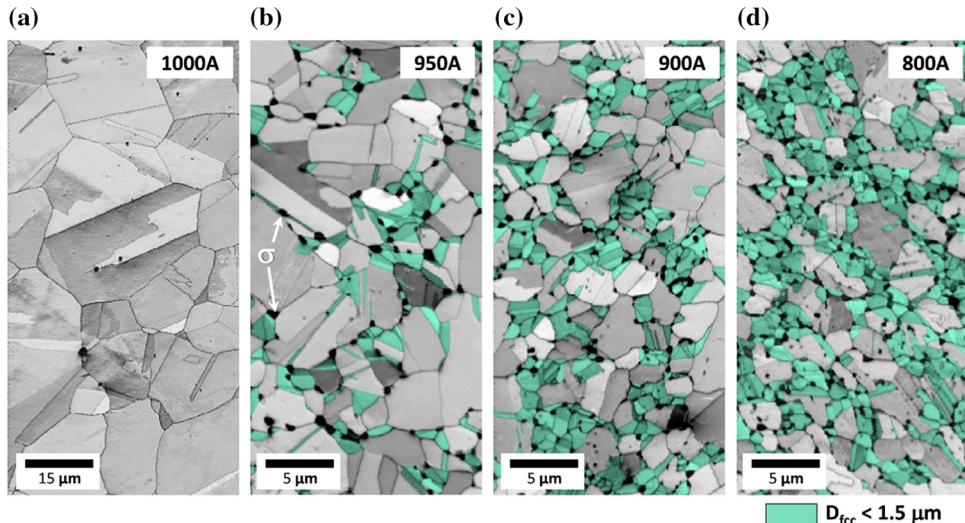


Figure 6 Microstructures of CoCrFeMnNi HEA: **a** starting; **b** 90% cold-rolled; **c** 90% cryo-rolled materials [31]. Reproduced from [31] with permission from Elsevier.

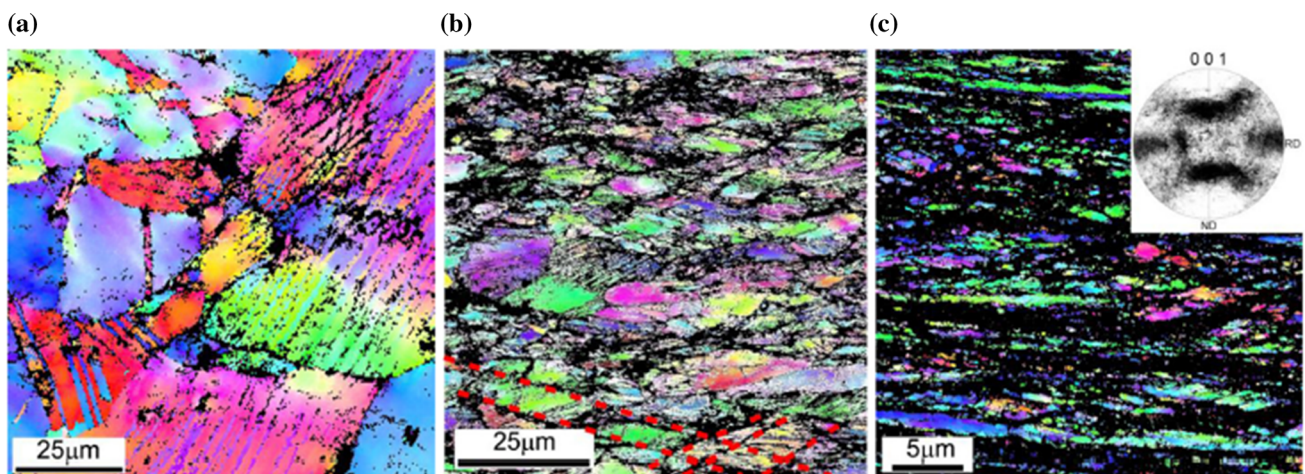
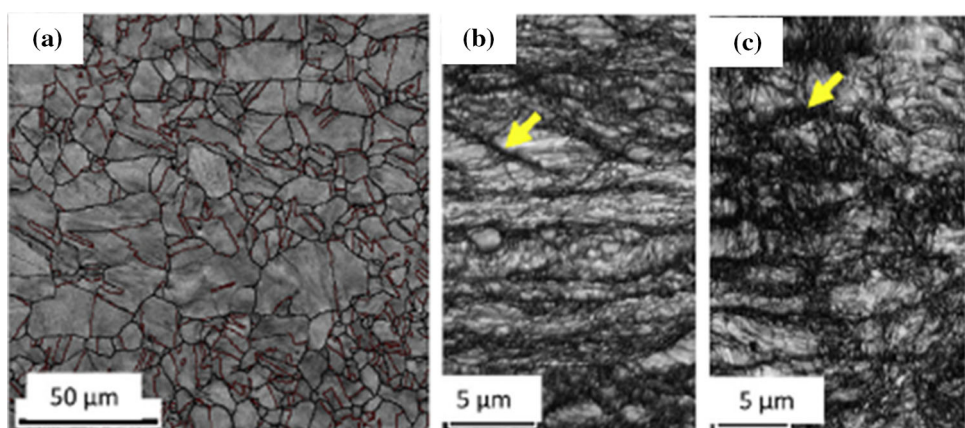
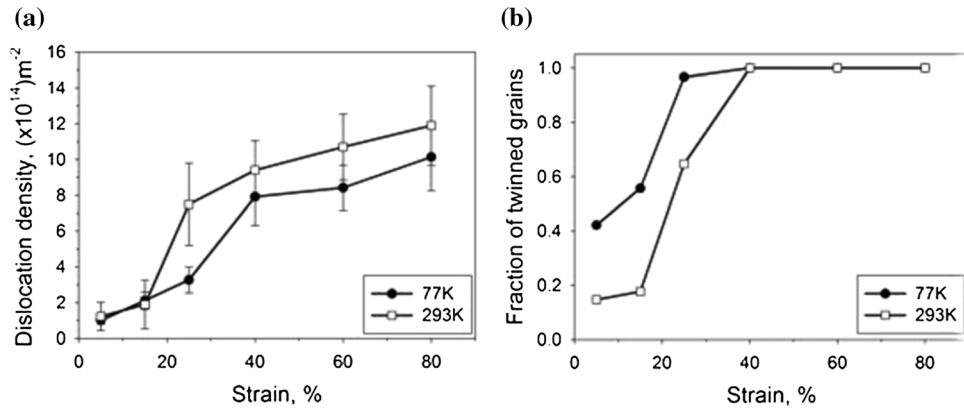


Figure 7 Normal-direction EBSD (inverse-pole-figure) maps taken on the transverse plane of CoCrFeNiMn rolled at 77 K: **a** 15%; **b** 40%; **c** 80% [72]. Reproduced from [72] with permission from Elsevier.

increase in cryo-rolling deformation, which can hinder the dislocation movement and improve mechanical properties at 77 K. The dislocation

density and the volume fraction of twins of rolling deformation at different temperatures are calculated as shown in Fig. 8. The dislocation density is higher

Figure 8 Microstructure of CoCrFeNiMn HEA with different strain at 293 or 77 K: **a** fraction of dislocation density; **b** twinned grains [72]. Reproduced from [72] with permission from Elsevier.



during room-rolling, and the fraction of twins is higher at the initial stages of deformation during cryo-rolling. It is further shown that the excellent mechanical properties at low temperature are related to the activated twins during deformation. The main deformation mechanism is dislocation slip at room temperature and twin deformation at low temperature.

The strengthening mechanism of the grain refinement is to hinder the movement of dislocations by the increasing grain boundaries. In traditional alloys, the relationship between yield strength and grain size is expressed by the Hall-Petch relation ($\sigma_{SY} = \sigma_0 + kd^{-1/2}$). For HEAs, the relationship between the yield strength and the size also complies with the Hall-Petch relationship at room temperature [73]. The relationship is applicable to the low-temperature deformation behavior of HEAs as have been studied. Otto et al. studied the tensile properties of CoCr-FeMnNi HEA with three different grain sizes (4.4, 50 and 155 μm) at different temperatures and found the yield strength increases with the decrease in grain size [40]. The Hall-Petch relationship between grain size and yield strength in CoCrFeMnNi HEA at different temperatures was studied, as shown in Fig. 9. Table 1 summarizes the intercept (σ_0) and slope values (k) in Fig. 9. The Hall-Petch slopes are found to range from 538 to 421 $\text{MPa}\cdot\mu\text{m}^{-1/2}$ for temperatures of 77 to 873 K, which is higher than that of FCC metals. Sun et al., respectively, prepared single-phase equiatomic CoCrFeMnNi HEA samples with smaller grain sizes of 0.65 μm (UFG), 2.1 μm (FG) and 105 μm (CG) by cold rolling and annealing treatment [74]. The results show that there is a linear relationship between the yield strength and the grain size at different temperatures Fig. 9 (d). The Hall-Petch slopes

of Cantor alloy with smaller grain sizes are higher as shown in Table 1, which suggests higher slip-transfer resistance at grain boundaries. The friction stress (σ_0) and k values of the alloy increase with the decrease in temperature, which indicates the temperature dependence for Hall-Petch strengthening. The ultra-fine-grained structure of annealed HEAs makes it have excellent strength and toughness compared with other structural materials. The study of grain refinement strengthening at low temperature not only provides a theoretical basis for improving mechanical properties, but also expands the application of UFG HEAs in low-temperature environments. The relationship between microstructures and properties of UFG materials has been further studied, which provides an attractive guideline for the preparation of UFG alloys with excellent low-temperature mechanical properties.

Effects of stacking fault energy on cryogenic temperature properties of HEAs

The improvement of the strength-ductility of the alloy is closely related to the deformation mode, such as dislocation sliding, deformation twinning and deformation-induced phase transition [75–77]. A large number of studies show that the stacking fault energy (SFE) significantly affects the deformation mode in HEAs. High SFE reduces the splitting distance of two partial dislocations to promote the dislocation slipping. Low SFE increases the distance of two partial dislocations to form stacking faults, which benefits deformation twinning and martensitic transformation [78, 79]. The twinning-induced

Figure 9 Hall–Petch relationship for the CoCrFeMnNi alloy at different temperatures: (a), (c) temperature dependence of 0.2% offset yield stress (σ_y); (b), (d) grain size dependence of 0.2% offset yield stress (σ_y) [40, 74]. Reproduced from [40] with permission from Elsevier. Reproduced from [74] with permission from Elsevier.

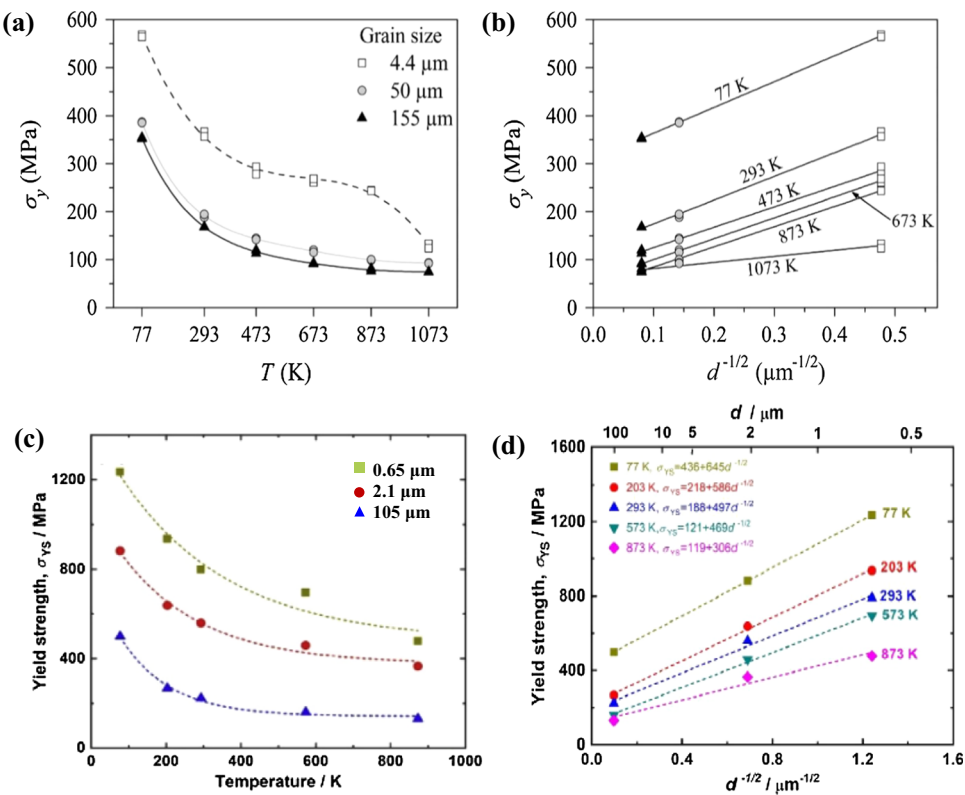


Table 1 Values of the Hall–Petch intercepts σ_0 and slopes k obtained from Fig. 9

Grain size(μm)	T(K)								Ref
	77	203	293	473	573	673	873	Ref	
$\sigma_0(\text{MPa})$	4.4,50,155	310	—	125	83	—	57	43	[40]
$k(\text{MPa}\cdot\mu\text{m}^{-1/2})$		538	—	494	425	—	436	421	
$\sigma_0(\text{MPa})$	0.6,2.1,105	436	218	188	—	121	—	119	[74]
$k(\text{MPa}\cdot\mu\text{m}^{-1/2})$		645	586	497	—	469	—	306	

plasticity (TWIP) and transformation-induced plasticity (TRIP) contribute to high strain hardening ability and delay the occurrence of necking. The composition of the alloy can significantly affect the SFE. SFE plays an important role in the improvement properties of HEAs at low temperature. Huang et al. calculated the stacking fault energy (SFE) of FeCrCoNiMn HEA at different temperatures and predicted the transformation of HCP phase at cryogenic temperatures by first principles calculations [80]. As shown in Fig. 10, the low temperature has a significant effect on SFE. The slope of SFE increases with the decrease in temperature, which indicates that SFE reaches a saturation state at high temperature. The calculated SFEs are $\sim 21 \text{ mJ/m}^2$ at room temperature and $\sim 3.4 \text{ mJ/m}^2$ near 0 K. Based on the

calculated results and experimental observations, it is found that the deformation mechanism of FeCrCoNiMn HEA is determined by SFE. The critical value of activation of the TWIP effect is $\sim 21 \text{ mJ/m}^2$ and the critical value of activation of the TRIP effect is $\sim 8 \text{ mJ/m}^2$, which is close to the SFE value of $10\text{--}18 \text{ mJ/m}^2$ in stainless steel [81–83]. SFE is determined as a function of temperature by first principles calculations and found to reduce with the decrease in temperature [84].

The atomic supercell arrangements of FCC structure HEAs are described by using the special quasi-random structure (SQS) technique, as shown in Fig. 11 [85–87]. The unstable stacking fault (USF) and intrinsic stacking fault (ISF) energies are calculated by Eq. (1). The SFE of FCC structure CoCrFeNi and

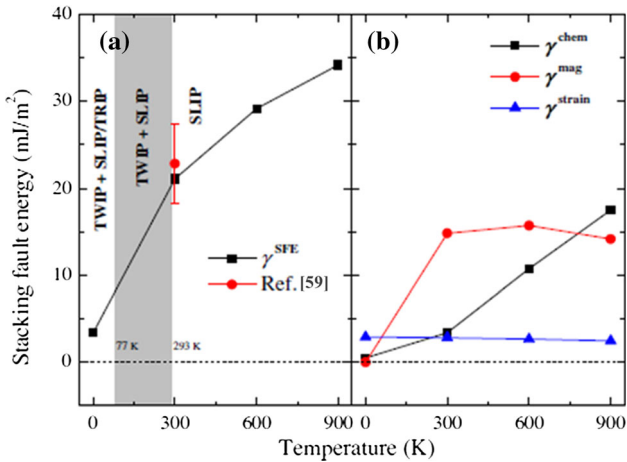


Figure 10 Theoretical SFE of FeCrCoNiMn HEA: **a** the total SFE $\gamma^{\text{SFE}} = (\gamma^{\text{chem}} + \gamma^{\text{mag}} + \gamma^{\text{strain}})$; **b** the individual contribution: chemical part γ^{chem} , magnetic part γ^{mag} and strain part γ^{strain} [80]. Reproduced from [80] with permission from Elsevier.

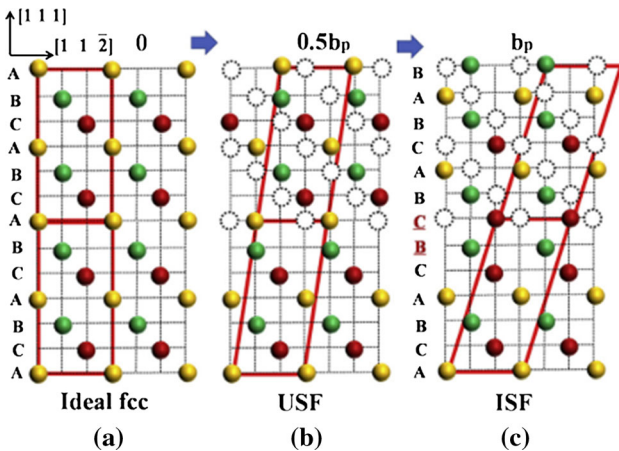


Figure 11 Schematic diagram of 6-layer fcc supercells: **a** ideal fcc, **b** unstable stacking fault (USF), **c** intrinsic stacking fault (ISF) [86]. Reproduced from [86] with permission from Elsevier.

Al_{0.57}CoCrFeNi HEAs with different SQS supercells is calculated by Eq. (1), as shown in Fig. 12 [86].

$$\gamma = \frac{E^{\text{sf}} - E^{\text{fcc}}}{A} \quad (1)$$

where E^{sf} represents the ISF or USF energy, E^{fcc} represents the energy of ideal FCC structure and A represents the area of supercell basal plane.

In addition to using simulation to calculate the SFE of HEAs, a large number of experimental methods are used to calculate the SFE of HEAs, including TEM and XRD methods. The experimental method can more easily obtain the parameters of SFE. The SFE of HEAs can be measured by observing the sizes of extended dislocation nodes or the width of partial dislocations in TEM images. SFE could be calculated, based on Eq. (2). The SFE of NiCoCr, FeNiCoCr and Fe₂₀Co₁₅Ni₂₅Cr₂₀Mn₂₀ HEAs measurements were taken by using weak-beam dark-field TEM as shown in Fig. 13 [88]. The partial dislocation core separation of NiCoCr is much wider and the calculated SFE is much lower than that of other HEAs.

$$\gamma = \frac{Gb_p^2}{8\pi d} \cdot \frac{2-v}{1-v} \left(1 - \frac{2v\cos 2\theta}{2-v}\right) \quad (2)$$

where γ is the SFE, G is the shear modulus, b_p is the magnitude of the partial Burgers vector, d is the separation distance, v is the Poisson's ratio, and θ is the angle between the dislocation and the Burgers vector of the full dislocation.

The SFE is calculated by XRD detection using Eqs. (3) and (4) [89–91]. Yang et al. calculated the SFE of the Fe₅₃Mn₂₉Co₉Cr₉ alloy and studied the effect of SFE on the deformation behavior of nano-twins at low temperature [92].

$$\gamma = \frac{K_{111}\omega_0 G_{(111)}a_0 A^{-0.37}}{\pi\sqrt{3}} \cdot \frac{\varepsilon^2}{\alpha} \quad (3)$$

$$\Delta 2\theta = \Delta(2\theta_{200} - 2\theta_{111}) \\ = -\frac{45\sqrt{3}}{\pi^2} \left(\tan \theta_{200} + \frac{1}{2} \tan \theta_{111} \right) \alpha \quad (4)$$

where $K_{111}\omega_0$ is the proportional constant of 6.6, $G_{(111)}$ is the shear modulus, a_0 is the lattice constant, A is constant related to the anisotropy of 3.43, ε is the micro-strain; α is the possibility of the stacking fault, and θ_{hkl} is the hkl plane in the XRD.

The SFE of alloys by the calculation of simulation and experiment methods at different temperatures is summarized in Table 2. It is found that the SFE is significantly affected by the alloy components and loading temperature. With the decrease in temperature, the SFE of the alloy decreases. The multi-component characteristics of HEAs have lower SFE, inducing a variety of deformation mechanisms and improving the properties, especially at low temperatures.

Figure 12 The SFE of CoCrFeNi and Al_{0.57}CoCrFeNi HEAs with different SQS supercells: (a), (b) USF energy, (c), (d) ISF energy [86]. Reproduced from [86] with permission from Elsevier.

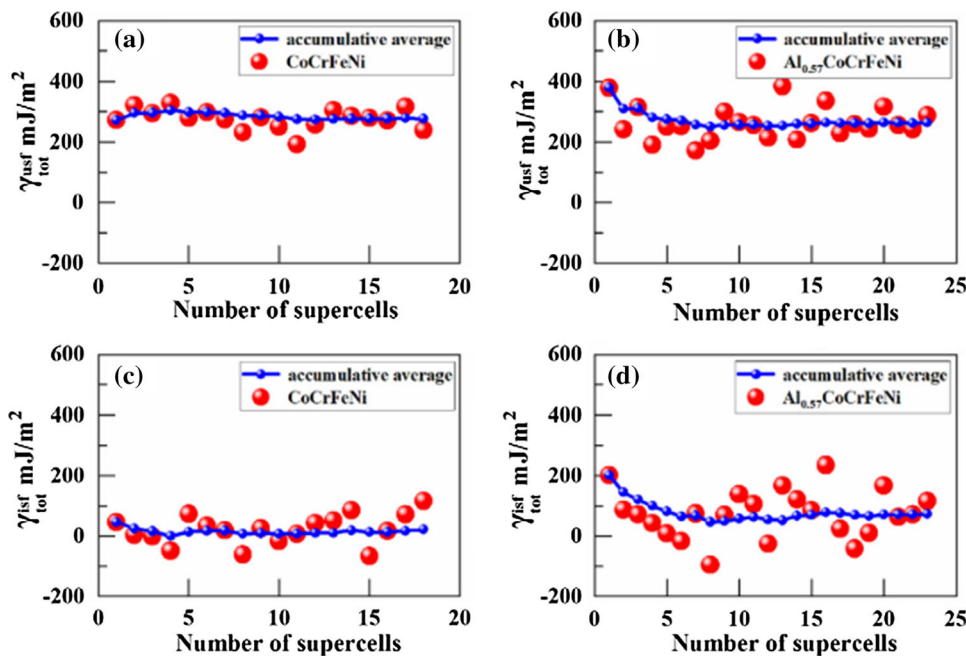


Figure 13 The TEM images of dissociated dislocations of HEAs: **a** NiCoCr, **b** FeNiCoCr, **c** Fe₂₀Co₁₅Ni₂₅Cr₂₀Mn₂₀, **d** SFE calculated and plotted by d as a function θ [88]. Reproduced from [88] with permission from Elsevier.

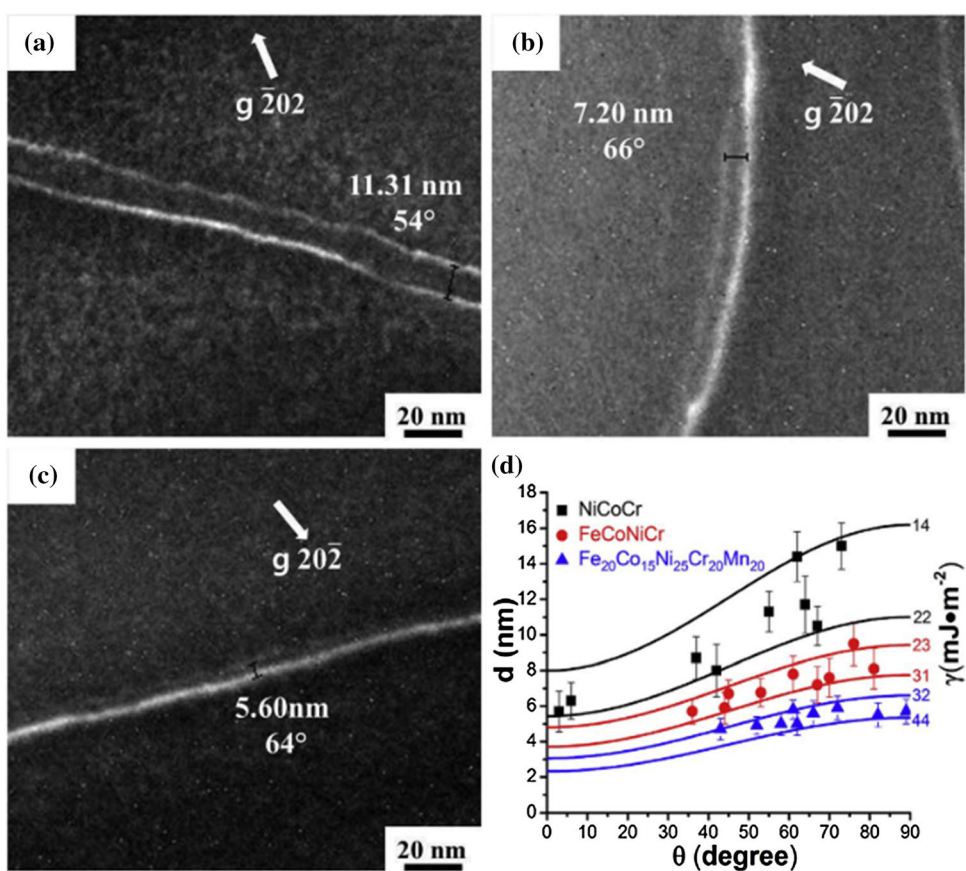


Table 2 The SFE of alloys calculated by experiment and simulation methods at different temperatures

Alloy	Method	SFE ($\text{mJ}\cdot\text{m}^{-2}$)	Temperature (K)	References
Ni	XRD	125	298	[93]
FeNi	XRD	105	298	[94]
FeNi	Calculation	100	298	[90]
FeNiCr	Calculation	60	298	[90]
CoCrNi	Calculation	-42.9	0	[95]
CoCrNi	Calculation	-24	0	[96]
CoCrNi	TEM	18–26	298	[97]
CoCrNi	TEM	14–22	298	[88]
CrCoNiFe	TEM	13	77	[98]
CrCoNiFe	XRD	7.4	140	[99]
CoCrFeNi	Calculation	21	298	[86]
CoCrFeNi	XRD	17–32	298	[100]
CoCrFeNi	TEM	23–31	298	[88]
CoCrFeMnNi	Calculation	3.4	0	[76]
CoCrFeMnNi	Calculation	18–27	298	[90]
CoCrFeMnNi	XRD	18–27	298	[100]
CoCrFeMnNi	TEM	25–35	298	[101]
CoCrFeNiMo _{0.2}	XRD	11	15	[47]
CoCrFeNiMo _{0.2}	XRD	17	77	[47]
CoCrFeNiMo _{0.2}	XRD	28	298	[47]
Fe ₄₀ Mn ₄₀ Co ₁₀ Cr ₁₀	TEM	19.5	173	[102]
Fe ₄₀ Mn ₄₀ Co ₁₀ Cr ₁₀	TEM	37.7	298	[102]
Fe ₂₀ Co ₂₃ Ni ₁₇ Cr ₂₀ Mn ₂₀	TEM	22–28	298	[103]
Fe ₂₀ Co ₂₇ Ni ₁₃ Cr ₂₀ Mn ₂₀	TEM	16–20	298	[103]
Al _{0.1} CoCrFeNi	TEM	26–34	298	[104]
Al _{0.57} CoCrFeNi	Calculation	73	298	[86]
Al _{0.6} CoCrFeNi	TEM	28.69	77	[49]
Al _{0.6} CoCrFeNi	TEM	49.33	298	[49]
Al ₂ CoCrFeMnNi	Calculation	3	0	[105]
Al ₂ CoCrFeMnNi	Calculation	5	100	[105]
Al ₂ CoCrFeMnNi	Calculation	8	200	[105]
Fe _{79.9} Mn ₁₈ C _{0.6} Al _{1.5} TWIP steel	Calculation	35	203	[106]
Fe _{79.9} Mn ₁₈ C _{0.6} Al _{1.5} TWIP steel	Calculation	49	298	[106]

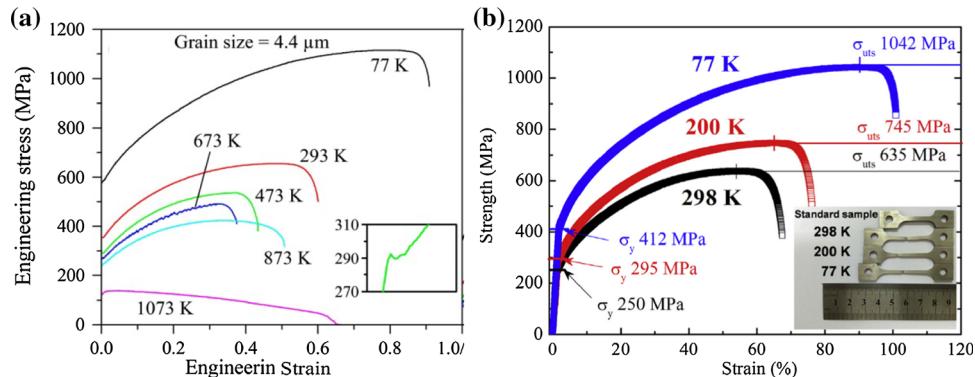
Mechanical properties of HEAs at cryogenic temperature

High-performance cryogenic materials can promote the development of aerospace, cryogenic liquid storage and underground pipeline transportation. At present steel is widely used in cryogenic temperature environments. Low-temperature steels are used below 273 K and cryogenic steels are used below 77 K. However, the segregation of components in steel affects its properties and application. These remarkable mechanical properties of HEAs make them a potential candidate for the wide cryogenic applications.

Tensile properties

The research of HEAs has gradually changed from the initial composition design to the performance optimization since the discovery of HEAs in 2004. In the traditional alloys, the ductility and toughness of structural materials often deteriorate in cryogenic temperature environments due to reduced damage-tolerance capacities or inherent crystallographic problems [107, 108]. It has been found that HEAs exhibit excellent strength–ductility combination at cryogenic temperature. Otto et al. performed a detailed study of the mechanical properties of CoCrFeMnNi HEA with special focus on the influence of temperature and microstructure [40]. At 77 K, the yield strength, tensile strength and elongation are

Figure 14 Representative engineering stress-strain curves at different temperatures: **a** CoCrFeMnNi alloy; **b** Al_{0.1}CoCrFeNi alloy [38, 40]. Reproduced from [40] with permission from Elsevier. Reproduced from [38] with permission from Elsevier.



600 MPa, 1100 MPa and 90%, respectively, which are 71%, 69% and 38% higher than those at room temperature, as shown in Fig. 14. The nanoscale deformation twins can provide an additional deformation mode to accommodate plasticity after interrupted tests at 77 K, but not in specimens tested at room temperature. This result has significance for the cryogenic temperature application of metal structural materials. Therefore, the strength–ductility combination effect of HEAs at cryogenic temperature has aroused many interests. Gludovatz et al. published an article entitled “a fracture resistant high-entropy alloy for genetic applications” in Science [6]. The tensile properties at cryogenic temperature and room temperature of CoCrFeMnNi HEA after cold rolling and annealing were further investigated. The mechanical properties actually are improved at cryogenic temperatures. At 77 K, the yield strength, tensile strength and fracture strain are about 750 MPa, 1300 MPa and 71%, respectively. After the publication of this paper, a large number of scholars have studied the cryogenic temperature properties of HEAs. The cryogenic temperature tensile properties of different HEA systems have been studied, and the micro-mechanism of strength–ductility at cryogenic temperature was further explored, which provides a theoretical basis for its application in cryogenic temperature structural materials. Li et al. studied the tensile properties of Al_xCoCrFeNi ($x = 0.1$ and 0.3) HEA prepared by hot forging at cryogenic temperatures and room temperature [38]. The fracture strength and strain of Al_{0.1}CoCrFeNi at 77 K are 1042 MPa and 81.6%, respectively. The fracture strength and strain of Al_{0.3}CoCrFeNi at 77 K are 1010 MPa and 75%, respectively. The results show that the strength and plasticity decrease with the increasing of temperature from 77 to 298 K.

Mechanical nano-twinning is the structural flow unit instead of planar slip of dislocations, which leads to property enhancement at cryogenic temperatures. The strength and plasticity decrease with the increase in Al content, which indicates the effect of alloying elements on cryogenic temperature properties of HEAs. The influence of non-metallic C, Si and B elements on the mechanical properties of HEAs has been studied at low temperature. He et al. studied a series of nitrogen-doped FeMnCoCr HEAs and found that Fe₄₉Mn₃₀Co₁₀Cr₁₀N₁ has excellent strength (yield strength: 1078 MPa; tensile strength: 1630 MPa) and maintains uniform elongation of 33.5% at 77 K, which were attributed to twinning and martensitic transformation [45]. C and Si elements are alloyed into FeMnCoCr and completely dissolved into the matrix to improve strength and plasticity [109]. The solid solution strengthening and twin strengthening effects are attributed to cause high strength of 907 MPa and plasticity of 69.6% at low temperature, respectively.

To further study the low temperature deformation behavior, researchers have explored the ultralow temperature properties of HEAs. Naeem et al. published a paper on the ultralow temperature properties of HEAs in Science Advances, entitled “cooperative deformation in HEAs at ultralow temperatures” [110]. The ultralow temperature (295 K, 140 K and 15 K) tensile properties of CoCrFeMnNi HEA were studied. The strength and ductility of the alloy are improved with the decrease in temperature. It should be noted that the fracture strength is 2.5 GPa and the strain is 62% at 15 K. The serrations appear beyond 21% and the trend of temperature fluctuations due to serrations is superimposed by in situ neutron diffraction measurements at 15 K, as shown in Fig. 15(a). The serrations characterized by a sharp load drop increase with the deformation,

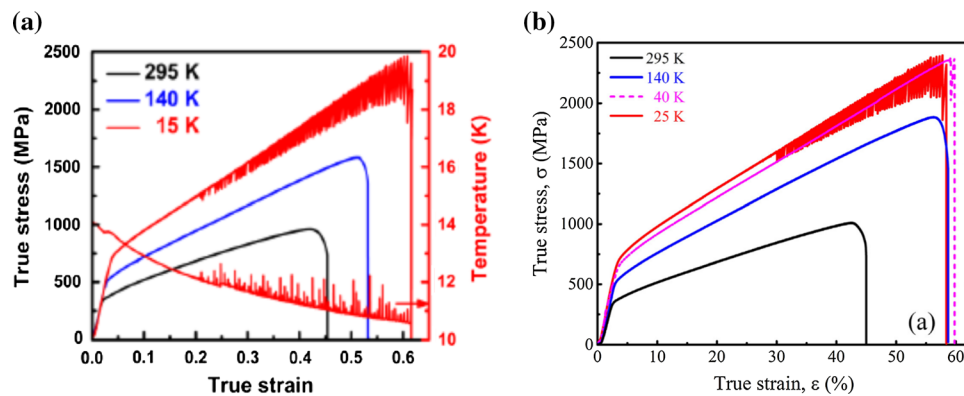


Figure 15 True stress–strain curves at ultralow temperatures: **a** CrMnFeCoNi alloy and the trend of temperature fluctuations (right-hand axis) due to serrations at 15 K, **b** CoCrFeNi [110, 111].

Reproduced from [110] with permission from AAAS (Author: Muhammad Naeem). Reproduced from [111] with permission from Elsevier.

approaching 570 MPa. The serrated deformation is attributed to the rapid development of SFs and twinning. The tensile curves of CoCrFeNi show that the yield strength increase from 331 to 676 MPa, the ultimate tensile strength increase from 1009 to 2396 MPa, and fracture strain are improved from 45

to 58.4% with lowering the temperature from RT to 25 K [111]. The massive serrations of CoCrFeNi HEA are also observed at 25 K when the stress is higher than 1600 MPa. The stress-drop becomes increasingly large with deformation, exceeding 300 MPa by the end, as shown in Fig. 15(b). These exceptional

Table 3 Cryogenic temperature tensile properties of different HEAs (Gs: grain size; T: temperature; σ_y : yield strength; σ_b : ultimate tensile strength; ε : fracture strain)

	Alloy	Condition	Gs/ μm	T /K	σ_y /MPa	σ_b /MPa	ε /%	Ref
CoCrFeMnNi	Cold-rolled, annealed			293	800	850	28	[74]
			0.65	203	950	1100	30	
				77	1210	1500	41	
				293	590	800	35	
			2.1	203	610	1000	48	
				77	850	1300	55	
				293	200	580	60	
			105	203	280	680	68	
				77	500	1000	83	
			5	293	604	835	44	[112]
	CoCrFePdNi	Cold-rolled, annealed		77	900	1244	60	
				135	293	410	710	56
				77	666	1012	74	
	CrFeCoNi	Hot-rolled, annealed		50	293	210	690	41
				77	435	1100	66	
	NiCoCrMn	Cold-rolled, annealed		36	293	300	700	42
				77	500	1100	65	[113]
			5–50	293	410	895	73	[5]
	NiCoCr	Cold-rolled, annealed		198	555	1060	67	
				77	657	1311	90	
				8.8	298	393	736	44
	$\text{Fe}_{40}\text{Ni}_{25}\text{Cr}_{15}\text{-Co}_{10}\text{V}_{10}$	Cold-rolled, annealed		77	613	1074	60	[114]
				20	298	500	900	60
	$\text{Al}_{0.3}\text{CoCrFeNi}$	Cold-rolled annealed + aging		77	700	1400	65	[115]

mechanical properties and multiple deformation pathways show great potential for the cryogenic temperature application of HEAs in the future.

The cryogenic temperature tensile properties of HEAs with different systems are summarized in Table 3. The results show that the properties of HEAs are strongly dependent on temperature. The tensile strength and plasticity of the investigated alloys increase with the decrease in temperature. This phenomenon is attributed to dynamic twinning or transformation-induced plasticity during deformation. The excellent low-temperature tensile properties of HEAs show great potential application of structural materials compared with other low-temperature materials such as low-temperature steels.

Compression properties

In order to expand the application range of HEAs at low temperature, researchers have also carried out many experiments on the compression deformation behavior of HEAs at low temperature and obtained many performance parameters with guiding significance. In this section, the compression properties of different systems of HEAs at cryogenic temperature are introduced.

Xia et al. studied the compressive characteristics of a single-phase FCC structure with the composition of $\text{Al}_{0.1}\text{CoCrFeNi}$ HEA at 298, 200 and 77 K, respectively [116]. The yield strength was 120 MPa, 168 MPa and 275 MPa for the alloy at different temperatures. When the compression tests were conducted up to the ~ 50% plastic strains, the alloy showed excellent properties at 77 K. Meanwhile, the

remarkable strain hardening ability and the serration phenomena were observed at 77 K. This is attributed to the additional deformation mechanism at cryogenic temperature, as shown in Fig. 16. The deformation mechanism was planar dislocation glide at 298 K and 200 K. The extensive nano-twins were detected at 77 K. The $\text{Ag}_{0.5}\text{CoCrCuFeNi}$ HEA has been found that the structure consists of a solid solution with an FCC lattice consisting of two phases with different chemical compositions. High strength and plasticity are well combined at room temperature [117]. Laktionova et al. studied the mechanical properties of the $\text{Ag}_{0.5}\text{CoCrCuFeNi}$ HEA with decreasing temperature from 300 to 4.2 K [118]. The yield strength increased from 450 MPa at 300 K to 750 MPa at 4.2 K. The alloy has excellent strength and plastic deformation ability. The serration phenomenon was observed at 4.2 K and 7.5 K.

Tabachnikova et al. studied several CoCrFeNiMnV_x ($x = 0, 0.25, 0.5, 0.75$) HEAs with different contents of the intermetallic phase in uniaxial compression at 4.2–300 K [119]. The yield strength of all samples increased with the decrease in compression temperature from 300 to 4.2 K as shown in Table 4. The different V content affects the compression properties of the alloy. The increase in V concentration promotes σ phase precipitation and growth in FCC grains. The plastic deformation of FCC phase occurs and σ phase hinders dislocation movement to improve strength. The atoms cluster and Peierls relief of HCP and BCC alloys are more strong barriers for thermally activated motion, which leads to a strong temperature dependence of strength. Thus, nano-crystalline materials are have ultrahigh cryogenic strength [120]. The cryogenic

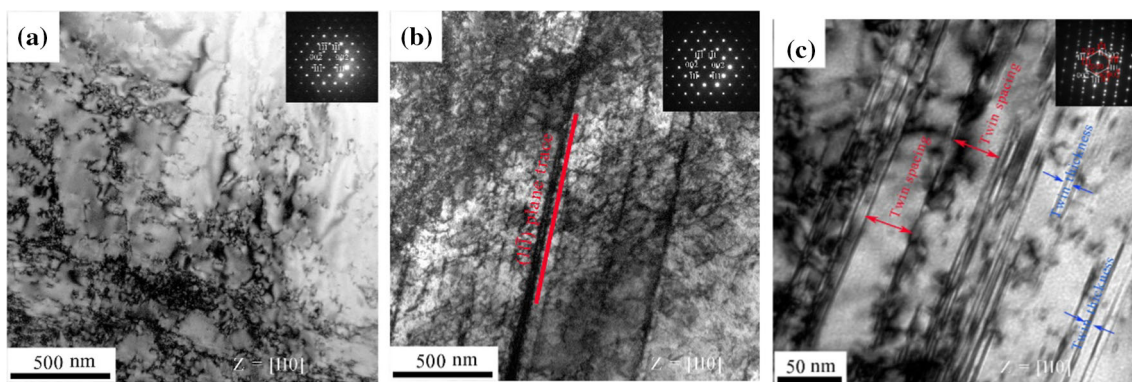


Figure 16 The microstructures of $\text{Al}_{0.1}\text{CoCrFeNi}$ HEA compressive: **a** 298 K; **b** 200 K; **c** 77 K [116]. Reproduced from [116] with permission from Elsevier.

Table 4 Cryogenic yield strength relation of as-solidified and annealed (1000 °C for 24 h) CoCrFeNiMnV_x HEAs in comparison with other materials [119]

Material	Microstructure	$\sigma_{0.2}/\text{GPa}[77 \text{ K}]$	$\sigma_{0.2}/\text{GPa}[300 \text{ K}]$
CoCrFeNiMn, as-solidified	FCC	0.43	0.23
CoCrFeNiMn, annealed	FCC	0.42	0.19
CoCrFeNiMnV _{0.25} , as-solidified	FCC	0.44	0.20
CoCrFeNiMn V _{0.25} , annealed	FCC + $\sigma(2\%)$	0.36	0.20
CoCrFeNiMn V _{0.5} , as-solidified	FCC + $\sigma(20\%)$	0.49	0.26
CoCrFeNiMn V _{0.5} , annealed	FCC + $\sigma(28\%)$	0.86	0.66
CoCrFeNiMn V _{0.75} , as-solidified	FCC + $\sigma(37\%)$	1.09	0.82
CoCrFeNiMn V _{0.75} , annealed	FCC + $\sigma(48\%)$	1.19	0.87
Ni, coarse-grained	FCC	0.07	0.058
Ni, nano-crystalline	FCC	1.24	0.84
Co, coarse-grained	HCP	0.39	0.27
Co, nano-crystalline	HCP	1.71	0.95

yield strength relation of CoCrFeNiMnV_x HEAs in comparison with other materials is shown in Table 4. The coarse grain CoCrFeNiMn and CoCrFeNiMnV_{0.25} HEAs have high cryogenic strength in comparison with traditional alloys. This is further explained that the unique crystal structure of HEAs is different from that of traditional alloys at low temperature.

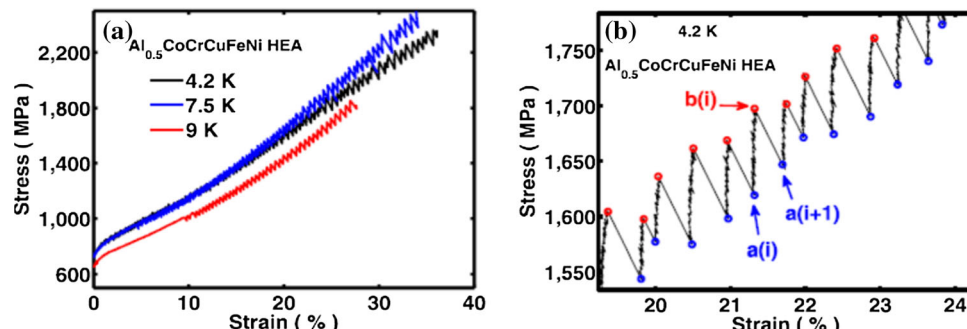
The HEAs have excellent mechanical properties and serrated flow phenomenon at ultralow temperature deformation. Guo et al. studied the uniaxial compression plastic behavior of the Al_{0.5}CoCrCuFeNi HEA at 4.2 K, 7.5 K and 9 K [121]. When strain was 20–30% at different temperature, tensile loading of the specimens was terminated. As shown in Fig. 17, it is found that the stress drops suddenly without fracture in the process of plastic deformation. Al_{0.5}-CoCrCuFeNi HEA has excellent compression properties and serrated flows occur in the temperature range. Guo et al. made statistical analysis of serration data and established as model analysis. The elastic energy is stored during a(i)-b(i) stage. The stress suddenly decreases to release the stored elastic energy during b(i)–a(i + 1) stage. The serration

behavior is characterized by the largest Lyapunov exponents (negative) at 4.2 K, 7.5 K and 9 K which are stable and ordered.

Fracture toughness

The excellent cryogenic temperature properties make the alloys show great potential application for cryogenic temperature. The fracture toughness of materials reflects the critical stress required for the fracture of materials due to the inherent defects (inclusions and micro-cracks) or structural defects (uneven thickness) existing in the alloys. Gludovatz et al. examined the damage tolerance of typical FCC structure FeCoCrNiMn HEA by testing compact tensile specimens with pre-cracks at ambient and cryogenic temperature [6]. The results show that mechanical properties of FeCoCrNiMn HEA are improved at cryogenic temperatures and fracture toughness values exceed 200 MPa·m^{1/2}, as shown in Fig. 18. Stereomicroscopic photographs of the fracture surfaces after testing indicate less lateral deformation and necking-like behavior with decreasing

Figure 17 The compressive stress-strain curves: **a** 4.2 K, 7.5 K and 9 K, **b** the amplified stress-strain curves at 4.2 K [121]. Reproduced from [121] with permission from AIP Publishing.



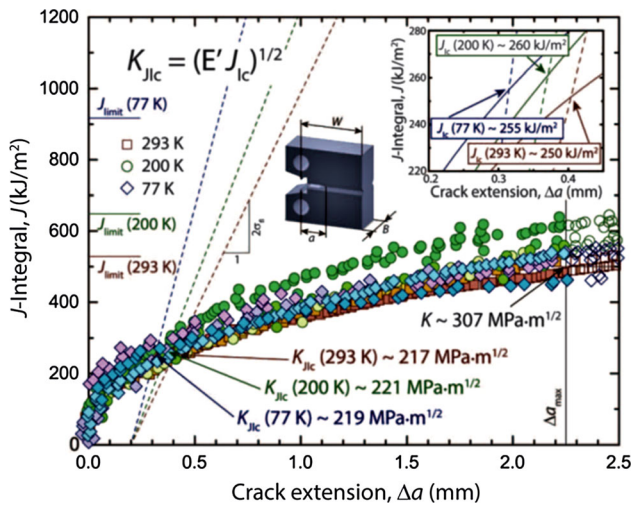


Figure 18 Fracture toughness tests of the FeCoCrNiMn HEA on compact tension [6]. Reproduced from [6] with permission from AAAS Publishing.

temperature. The sample has more distorted crack paths at 77 K and absorbs more fracture energy, which leads to excellent fracture toughness. Gludovatz et al. examined the fracture toughness of an equiatomic medium-entropy alloy containing only three elements, CrCoNi by the same method at 293 K, 198 K and 77 K [5]. The results show that the alloy exhibits similar results with FeCoCrNiMn and has a fracture toughness value above $200 \text{ MPa}\cdot\text{m}^{1/2}$. The fracture toughness of CrCoNi alloy increases from $207.7 \text{ MPa}\cdot\text{m}^{1/2}$ at 298 K to $273.3 \text{ MPa}\cdot\text{m}^{1/2}$ at 77 K. CrCoNi medium-entropy alloy exhibits excellent strength and toughness combination, compared to

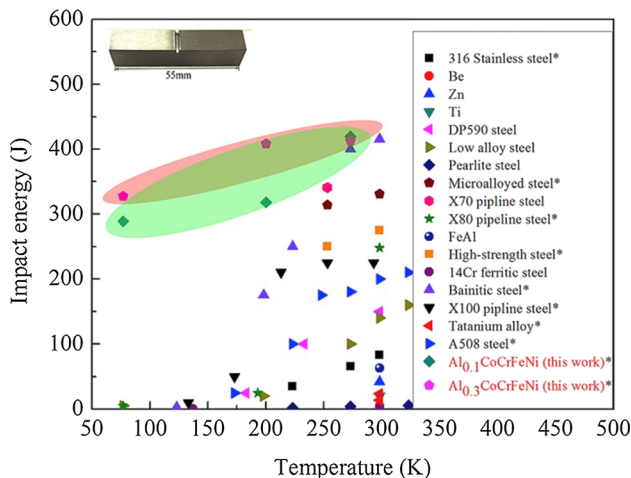


Figure 19 Summary of the Charpy impact energy of materials at the different temperatures [38]. Reproduced from [38] with permission from AAAS Publishing.

certain austenitic stainless steels, high-Ni steels, and other high- and medium-entropy alloys reported to date [5].

The Charpy impact energy measurements of Al_x-CoCrFeNi HEAs with V-type notch were carried out at different temperatures by Li et al. [38]. The low-temperature impact toughness of Al_{0.1}CoCrFeNi and Al_{0.3}CoCrFeNi HEAs is summarized with other conventional alloys, as shown in Fig. 19. The results show that the Charpy impact energy of the Al_{0.1}-CoCrFeNi alloy is above 289 J at 77 K and the value of the Al_{0.3}CoCrFeNi alloy is approximately 328 J at 77 K. The alloys with outstanding fracture resistance are candidates for extremely cold environment structure materials. The property enhancement is probably due to the fact that mechanical nano-twinning is the structural flow unit instead of planar slip of dislocations. However, the precise nature also deserves a study in the future.

Representative FCC HEAs or medium-entropy alloys have drawn a lot of attention due to the excellent damage tolerance at cryogenic temperature. Jo et al. investigated non-equiautomatic fracture toughness of V₁₀Cr₁₀Fe₄₅Co₂₀Ni₁₅ HEA by testing compact tensile specimens at 298 K and 77 K [122]. The K_{Jc} fracture toughness values are 219 and 232 $\text{MPa}\cdot\text{m}^{1/2}$ at 298 and 77 K, respectively. The in situ nano-oxide-reinforced CoCrFeMnNi HEA has ultrastrong cryogenic strength of 1.45 GPa and superior impact toughness by laser powder bed fusion [123]. The excellent fracture toughness results from the absence of twins at 298 K and the increased propensity to twin formation at 77 K. It is further explained that the high fracture toughness at low temperature is mainly related to the appearance of twins. In general, the propensity for twin formation is affected mainly by the SFE. It is well known that deformation mechanisms are experienced in the order of slip, TWIP and HCP TRIP as the SFE decreases [124]. Jo et al. further employed the Ab initio calculations to understand the SFEs of three different multi-principal element alloys (MPEAs): V₁₀Cr₁₀Fe₄₅Co₂₀Ni₁₅, CrMnFeCoNi, and CrCoNi as shown in Table 5 [122]. Deformation mechanisms varied with the SFE of FCC phase and test temperature in the V₁₀Cr₁₀Fe₄₅Co₂₀Ni₁₅, CrMnFeCoNi, and CrCoNi alloys are schematically illustrated in Fig. 20. The CrCoNi alloy have the lowest SFE, so the twin and HCP lamella deformation are expected to be easier than in the other alloys with

Table 5 Room- and cryogenic-temperature (298 and 77 K) fracture toughness test results and SFE estimated from the Ab initio calculation of the V₁₀Cr₁₀Fe₄₅Co₂₀Ni₁₅, CrMnFeCoNi and CrCoNi MPEAs [5, 6, 125]

Test temperature(K)	Alloy	Fracture toughness K _{Jlc} (MPa·m ^{1/2})	Stacking fault energy (mJ·m ⁻²)
298	V ₁₀ Cr ₁₀ Fe ₄₅ Co ₂₀ Ni ₁₅	219	63.5
	CrMnFeCoNi	217	30
	CrCoNi	208	22
77	V ₁₀ Cr ₁₀ Fe ₄₅ Co ₂₀ Ni ₁₅	232	—
	CrMnFeCoNi	219	—
	CrCoNi	273	—

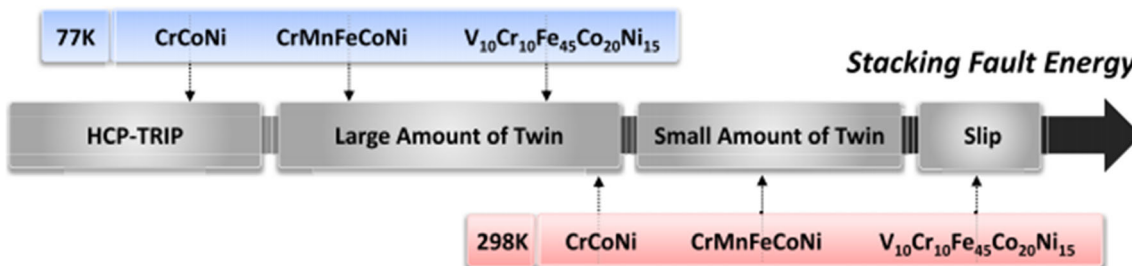


Figure 20 Schematic illustration of deformation mechanisms varying with the SFE and test temperature for the V₁₀Cr₁₀Fe₄₅Co₂₀Ni₁₅, CrMnFeCoNi and CrCoNi alloys [122]. Reproduced from [122] with permission from Elsevier.

higher SFE at 77 K. Therefore, higher fracture toughness is expected in the CrCoNi alloy [5].

Deformation mechanisms of HEAs at cryogenic temperature

In conclusion, the HEAs have excellent comprehensive properties of tensile, compression and fracture toughness at low temperature. The HEAs exhibit excellent strength–ductility combination at cryogenic temperature, which is different from the characteristics of traditional alloys. Therefore, HEAs have great potential application as cryogenic temperature structural materials. At present, a large number of studies have explored the deformation mechanism of HEAs at low temperature [126–128]. Low SFE at low temperature is the key to induce the deformation mechanism. The relationship between SFE and deformation mechanism is reflected by calculation and experiment: dislocations slip (SFE > 60 mJ·m⁻²); twinning (20 < SFE < 60 mJ·m⁻²); phase transformation (SFE < 20 mJ·m⁻²) [124, 129–131].

Defect evolution mechanisms of HEAs during deformation at cryogenic temperature

The mechanical properties of materials are closely related to the evolution of micro-defects (dislocations, twins, vacancies and short-range order (SRO)) during deformation. The HEAs with unique component characteristics have crystal structure, so there are a lot of micro-defects which affect its deformation behavior. It is of great significance to establish the physical model of strengthening mechanism and fracture behavior and to develop strength–plasticity combination materials for HEAs by exploring the evolution of micro-defects during low-temperature deformation.

HEAs with the concept of multi-component design lead to large lattice distortion, which realizes solid solution strengthening, especially at low temperature. The strengthening effect is commonly folded into the lattice friction part. The lattice friction stress (σ_{fr}) of HEAs can be calculated by Eq. (5) [113].

$$\sigma_{fr} = \sigma_p(0) * \exp\left(\frac{-T}{C}\right) \quad (5)$$

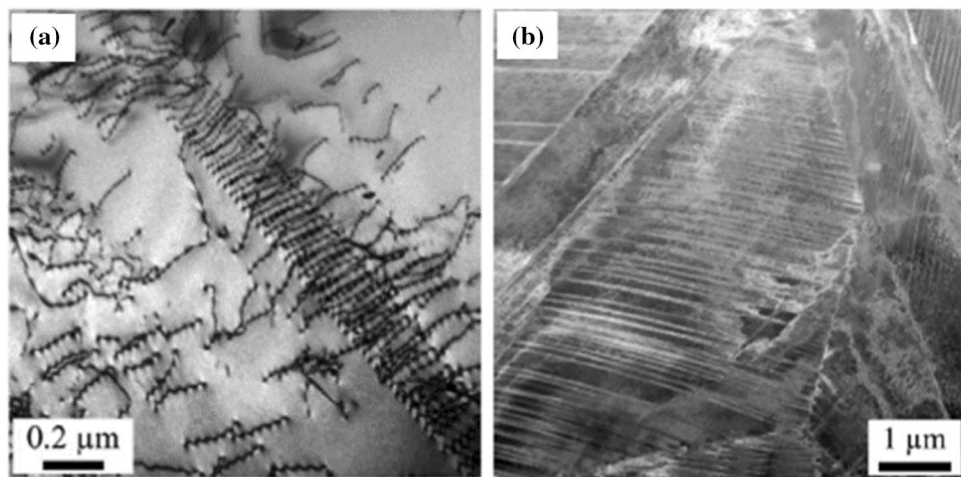
where $\sigma_p(0)$ is the Peierls stress at 0 K, T is the loading temperature, and C is a constant. According to Eq. (5), the σ_{fr} is temperature-dependent and increases with the decrease in loading temperature. Wang et al. reported a large yield strength of $\text{Fe}_{40.4}\text{-Ni}_{11.3}\text{Mn}_{34.8}\text{Al}_{7.5}\text{Cr}_6$ doped with 1.1 at.% C HEAs at 77 K, which is attributed to the lattice friction stress [132]. Large lattice friction stress causes a larger critical resolved stress to nucleate the dislocation [133].

Otto et al. studied the deformation mechanism of CoCrFeMnNi HEA at 293 and 77 K by TEM [40]. The results show that there are two deformation mechanisms (dislocation slip and twin deformation) in the alloy at 77 K, while there is only dislocation slip mechanism at room temperature. As shown in Fig. 21 (a), complete $1/2 < 110 >$ -type dislocations are decomposed into $1/6 < 112 >$ Shockley partial dislocations during deformation. Nano-twins caused by deformation are found for a sample strained to 20.2% at 77 K, as shown in Fig. 21 (b). The activation of twins introduces new interfaces and reduces the free path of dislocation movement in the tensile process. Twinning induced by low stacking fault energy in FCC structure results in a high work hardening ability and high tensile strength–plasticity in HEAs. Gludovatz et al. found that the high fracture toughness of CoCrFeMnNi HEA is also related to twins at cryogenic temperature [6].

The decrease in thermal activation strength not only increases the difficulty of defect activity, but also affects the competition between dislocation slip and deformation twins as the main deformation mechanism at low temperature. Ding et al. studied the deformation behavior and micro-deformation mechanism of

CrCoNi , CrMnFeCoNi and CrFeCoNiPd alloys by in situ straining in the transmission electron microscope at 93 K [134]. The dynamic deformation process of deformation twins at 93 K is shown in Fig. 22. The results show that the primary twins nucleate from the grain boundary, and then, the twin tip propagates along the Burgers vector of the $1/6 [21_1]$. The dislocations emitted from the primary twin boundary slide on the conjugate $\{111\}$ slip planes, forming secondary twins with the increase in strain. The formation of primary and secondary nano-twins effectively divides the original coarse grains ($\sim 130 \mu\text{m}$) into smaller subgrains. Another special twin with tetrahedral structure is observed in a cold-drawn CoCrFeNi HEA at 77 K [135]. Tetrahedral twins would lead to stress concentrations and cause incompatibility between the tetrahedron and the matrix by hindering the movement of dislocations, which induces severe work hardening. In addition, other plastic deformation mechanisms have cooperation effects, including partial dislocations and full dislocations slip, and a large number of cross-slip and multiple slip activated by the interaction between dislocation and grain boundary. The deformation-induced SRO structure causes severe lattice distortion, which improves the interface cohesion of HEAs via interfacial segregation at low temperatures. Jae et al. reported that the non-equiautomic $\text{Fe}_{40}\text{Mn}_{40}\text{Co}_{10}\text{Cr}_{10}$ and $\text{Ni}_{20}\text{Fe}_{20}\text{Mn}_{20}\text{Co}_{20}\text{-Cr}_{20}$ alloys by boron doping exhibited a notable yield strength at 77 K [48]. The SRO strengthening effect is attributed to the consecutive dislocations undergoing large resistance on the same glide planes in the boron-doped HEAs. These deformation mechanisms play a strengthening role and improve the cryogenic temperature properties of the alloys.

Figure 21 Representative TEM BF micrographs from the gauge sections of interrupted tensile test specimens of CoCrFeMnNi alloy after tensile strains at 77 K: **a** 2.4%, **b** 20.2% [40]. Reproduced from [40] with permission from Elsevier.



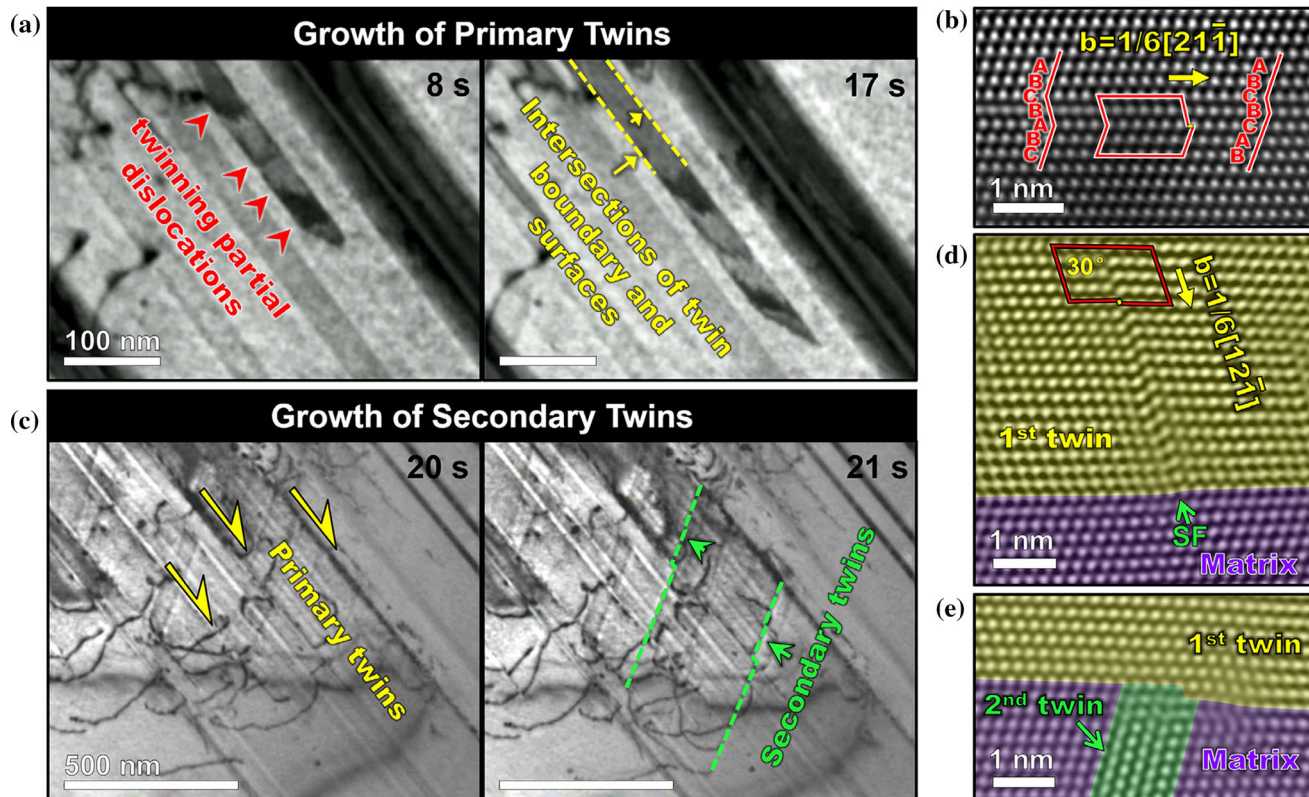


Figure 22 TEM images of twinning deformation in the CrFeCoNiPd alloy at 93 K: **a** the process of formation of a primary twin, **b** filtered atomic-resolution HAADF STEM image of a growing twin with viewing direction along $<110>$, **c** the initial stage of the nucleation of secondary twins, **d** atomic

structure of a partial dislocation emitted from a primary twin boundary, **e** filtered high-resolution HAADF-STEM image of the intersection between the primary and secondary twins [134]. Reproduced from [134] with permission from Elsevier.

The coexistence of multiple deformation mechanisms of HEAs at low temperature has competition and synergy. Stacking faults are very important in low-temperature deformation [80, 90]. Low stacking faults can cause entropy and lattice instability of the HEAs, thus reducing the activation stress of twins. The deformation twin formation increases grain boundaries to play a strengthening role. During deformation, twin nucleation is easier to nucleate at the defect position. Twin nucleation needs to overcome the critical stress, which is calculated according to Eq. (6) [136]. The twin boundary strengthening can be determined by using Eq. (7) [137–139].

$$\tau_{tw} = \frac{2\gamma_{isf} + 2\gamma_{csf}}{2b_p} \quad (6)$$

where γ_{isf} is the intrinsic SFE, γ_{csf} is the complex SFE of precipitate, and b_p is the Burgers vector of the Shockley partial dislocation

$$\Delta\sigma_{TB} = V_f k_t \lambda'^{-1/2} \quad (7)$$

where V_f is the volume fraction of twins, k_t is the strengthening factor by twin boundaries, and λ' is the space of twins.

Phase composition evolution mechanisms of HEAs during deformation at cryogenic temperature

In addition to the above-mentioned twinning-induced plasticity (TWIP), a large number of studies have introduced deformation-induced martensitic transformation (TRIP) in traditional alloy materials into HEAs. The lower stacking faults induce HCP transformation in the HEA at ultralow temperature. The SFE of HEAs is strongly dependent on temperature. The SFE of FeCoCrNiMo_{0.2} HEA dropped from 28 mJ·m⁻² at 293 K to 11 mJ·m⁻² at 15 K, which leads

to the martensite phase transformation [47]. The stress-induced phase transformation occurs in the process of deformation to improve the plastic deformation ability and achieve the purpose of strength-ductility combination by adjusting the composition of HEAs to reduce the stability of solid solution phases and SFE [11, 140–143]. The SFE (γ_{SFE}) of deformation-induced phase transformation is expressed as Eq. (8) [144].

$$\gamma_{SFE} = 2\rho\Delta G^{fcc \rightarrow hcp} + 2\sigma^{fcc/hcp} \quad (8)$$

where ρ is the molar surface density along the {111} planes, $\Delta G^{fcc \rightarrow hcp}$ is the free energy for $fcc \rightarrow hcp$ transformation, and $\sigma^{fcc/hcp}$ is the fcc/hcp interfacial energy. The $\Delta G^{fcc \rightarrow hcp}$ value is a function of temperature and decreases with the increasing of temperature. The thermodynamic driving force for phase transformation increases at low temperature.

Lin et al. studied the microstructure evolution of FeCoCrNi HEA during tensile deformation at 293 K, 77 K and 4.2 K and explored the transformation process from FCC phase to HCP phase at cryogenic temperature [145]. The micro-deformation mechanism is reflected from the experimental view, as

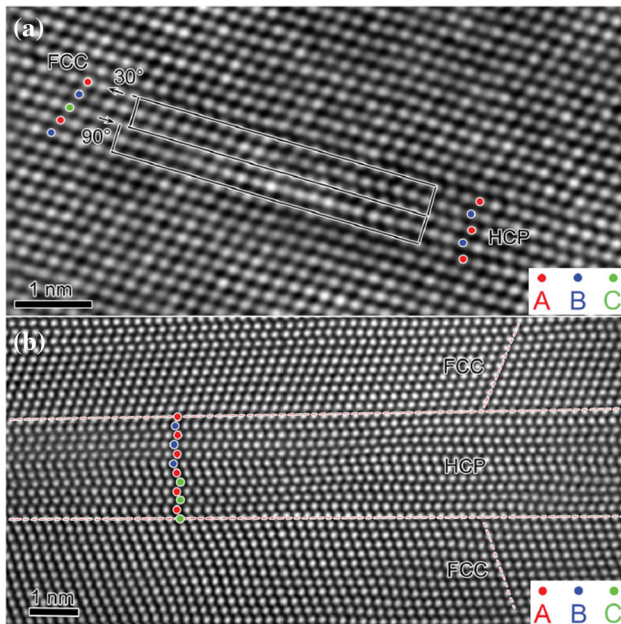


Figure 23 High-resolution HAADF STEM image: **a** A $[38]_{FCC}/[12_10]_{HCP}$ of FCC transforming to HCP, **b** 12 layers of HCP stacking including ABAB and ACAC sequences [145]. Reproduced from [145] with permission from Taylor Francis (Author: Qingyun Lin).

shown in Fig. 23. The results show that the Shockley partial dislocations slide along the Burgers vectors of $<112>/6$ on other {111} FCC planes to form the HCP phase. There are two kinds of adjacent Burgers circuits (a 30° Shockley partial and a 90° Shockley partial) in the deformation region and these two stacking faults can coexist, as shown in Fig. 23(a). As shown in Fig. 23(b), the 12-layer HCP lamella structure consists of 6-layer ABAB atom stacks and 6-layer of ACAC atom stacks, which further indicates that low SFE is the key factor leading to the TRIP effect. The microstructure of materials is closely related to its composition. The CoCrNi medium-entropy alloy is reported to have a higher mechanical strength and plasticity at cryogenic temperatures, which is attributed to nanostructured laminate twins and ϵ -martensite formation [146, 147]. Tirunilai et al. found that CoCrNi medium-entropy alloy showed a sandwiched structure by deformation twins, ϵ -martensite and matrix at 8 K, as shown in Fig. 24 [148]. The CoCrNi medium-entropy alloy has lower SFE and the twinning stress is reached earlier (at lower strains) at cryogenic temperatures [197].

The TRIP effect of HEAs during low-temperature deformation can not only realize the transformation from FCC to HCP, but also from FCC to BCC at certain conditions by changing the type and quantity of HEA components [149]. Song et al. studied the TRIP phenomenon of $V_{10}Cr_{10}Fe_{45}Co_{35}$ HEA with metastable FCC at room temperature and cryogenic temperature by quasi-static (strain rate: $10^{-3} s^{-1}$) and dynamic (strain rate: $3000 s^{-1}$) compression experiments [150]. As shown in Fig. 25, HCP phases are formed and grow from the FCC matrix during deformation, while all BCC phases are formed by transformation of formed HCP phases at the cryogenic temperature. With the increase in strain, a large amount of BCC phases is activated, whereas that of HCP phase decreases gradually, and the volume fraction of total (HCP + BCC) phase remains unchanged in $V_{10}Cr_{10}Fe_{45}Co_{35}$ HEA, as shown in Fig. 26. The volume fraction of BCC phases at cryogenic temperature is significantly higher than that at room temperature, which further indicates that BCC is more stable at cryogenic temperature. The TRIP effect results in a very high strain-hardening rate and consequently maximum compressive strength of more than 1.6 GPa. The FCC to BCC TRIP can markedly improve the properties of the HEA.

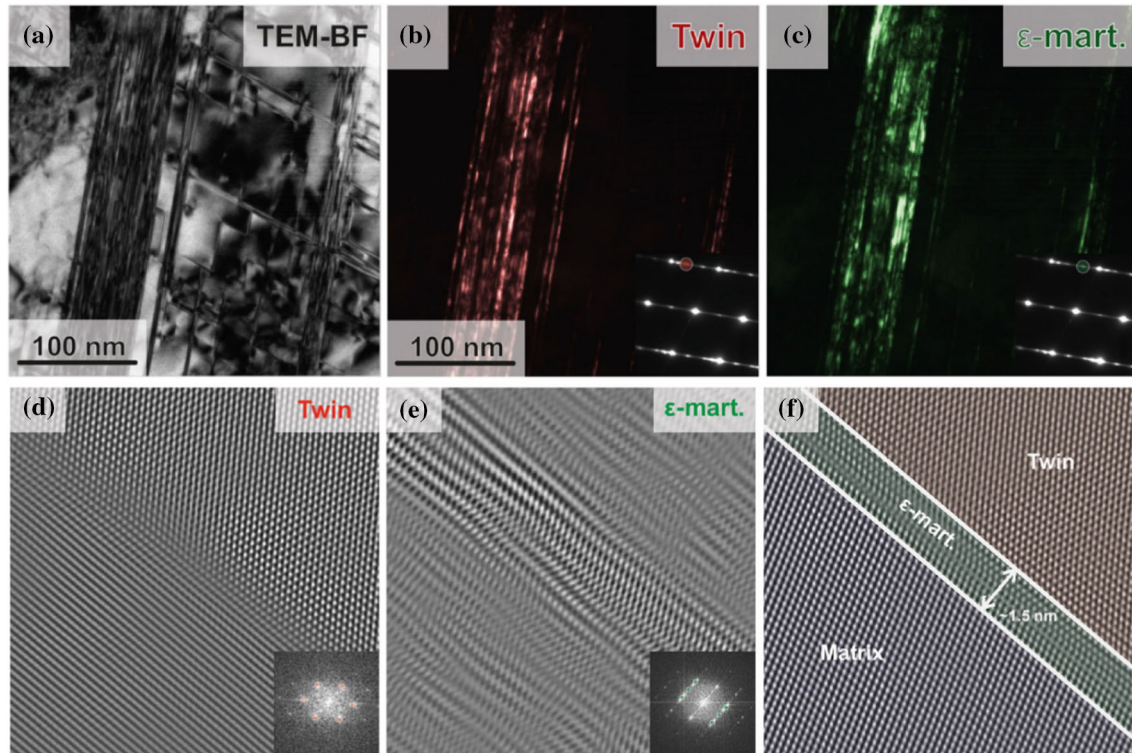


Figure 24 CoCrNi medium-entropy alloy deformed at 8 K: **a** TEM-BF image, **b** deformation twins using (1_1)1-entropy alloy deformed at 8 K: **a** TEM-BF image, **b** deformation twins using (1_1)1-entropy alloy deformed at 8 K: **a** TEM-BF image, **b** deformation twins using (1_1)18 K: **a** TEM-BF image, **b** deformation twins using (1_1)1-entropy alloy deformed at 8 K: **a** TEM-BF image, (b) deformation twins using (1_1)1-entropy alloy deformed at 8 K: **a** TEM-BF image, **b** deformation twins using (1_1)18 K: **a** TEM-BF image, **b** deformation twins using (1_1)1-entropy alloy deformed at 8 K: **a** TEM-BF image, **b** deformation twins using (1_1)1-entropy alloy deformed at 8 K: **a** TEM-BF image, **b** deformation twins using (1_1)1-entropy alloy deformed at 8 K: **a** TEM-BF image, **b** deformation twins using (1_1)18 K: (a) TEM-BF image, (b) deformation twins using (1_1)1-entropy alloy deformed at 8 K: (a) TEM-BF image, (b) deformation twins using (1_1)1-entropy alloy deformed at 8 K: (a) TEM-BF image, (b) deformation twins using (1_1)1-entropy alloy deformed at 8 K: (a) TEM-BF image,

Serration flow behavior of HEAs during deformation at cryogenic temperature

At 77 K, the deformation mechanism of HEAs is dislocation slip, twin activation and/or martensitic transformation. In addition to the deformation mechanisms, the serrated flow deformation mechanism is activated at ultralow temperature (such as liquid helium temperature). Serration deformation generally reduces the plasticity of materials [151, 152]. Different deformation mechanisms depend

(b) deformation twins using (1_1)18 K: (a) TEM-BF image, (b) deformation twins using (1_1)1-entropy alloy deformed at 8 K: (a) TEM-BF image, (b) deformation twins using (1_1)1-entropy alloy deformed at 8 K: (a) TEM-BF image, (b) deformation twins using (1_1)18 K: (a) TEM-BF image, (b) deformation twins using (1_1)1-entropy alloy deformed at 8 K: (a) TEM-BF image, (b) deformation twins using (1_1)18 K: (a) TEM-BF image, (b) deformation twins using (1_1)1-entropy alloy deformed at 8 K: (a) TEM-BF image, (b) deformation twins using (1_1)1-entropy alloy deformed at 8 K: (a) TEM-BF image, (b) deformation twins using (1_1)1-twin, (c) ε -martensite using (0_110) $_{\varepsilon}$ mартенсит, (d)-(e) high-resolution image [148]. Reproduced from [148] with permission from Elsevier.

on the composition and microstructure of the alloy. The serration flow behavior of HEAs is common, especially at extreme low temperatures. The discontinuous plastic flow lies in the thermomechanical coupling during deformation. Moon et al. reported that the medium-entropy alloy, $\text{Co}_{17.5}\text{Cr}_{12.5}\text{Fe}_{55}\text{Ni}_{10}\text{-Mo}_5$ (at.%) at 0.5–4.2 K exhibits discontinuous plastic deformation (DPF) and deformation-induced martensitic transformation [43]. The DPF phenomenon occurs at a critical temperature (T_c). The deformation by dislocation motion-induced heat release accelerates the rate of the plastic flow above

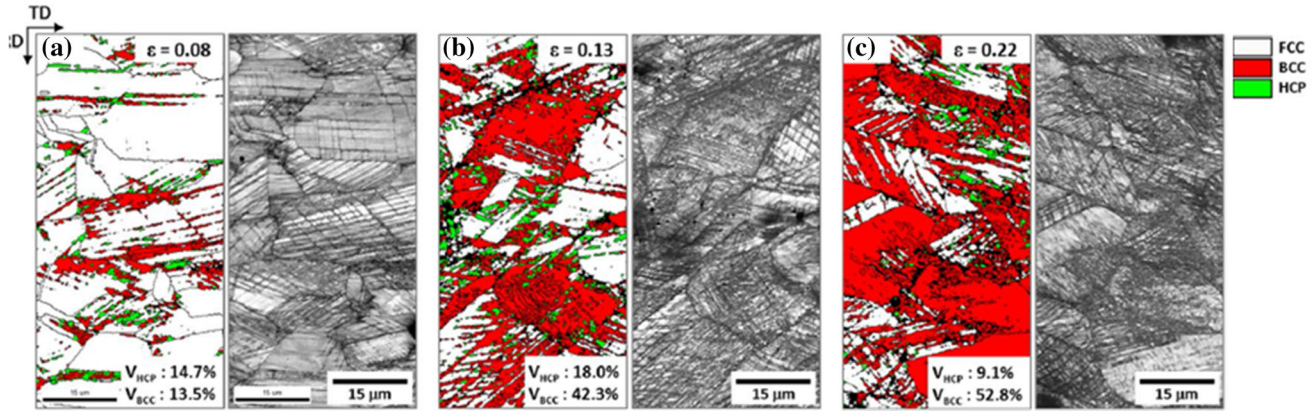


Figure 25 EBSD phase and IQ maps of the cross-sectional area of the quasi-statically compressed $V_{10}Cr_{10}Fe_{45}Co_{35}$ HEA specimen at true strains: **a** 0.08, **b** 0.13, **c** 0.22 [150]. Reproduced from [150] with permission from Springer Nature (Author: Hyejin song).

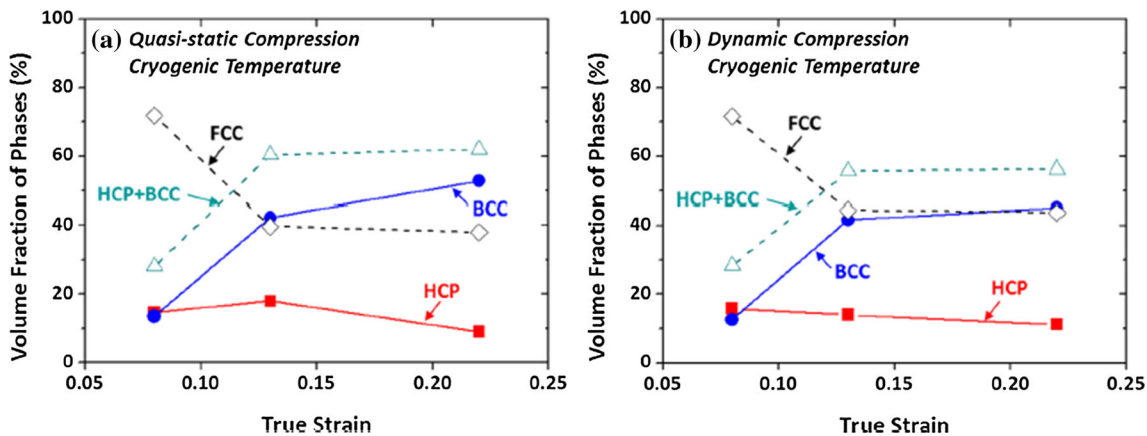


Figure 26 Volume fractions of FCC, BCC and HCP phases as a function of compressive true strain in $V_{10}Cr_{10}Fe_{45}Co_{35}$ HEA at cryogenic temperature: **a** quasi-statically compression, **b** dynamic

compression [150]. Reproduced from [150] with permission from Springer Nature (Author: Hyejin song).

T_c . Below T_c , the cross-slip of screw dislocation are inhibited due to the insufficient thermal energy, which causes the accumulation of dislocations at local barriers. The dislocations break away from barriers in discontinuous fashion, which induces serration flow during plasticity deformation. The μ precipitates and BCC martensite affect DPF by providing sites for strain localization [153]. Naeem et al. studied the deformation of CrMnFeCoNi HEA at ultralow temperature (15 K, 140 K, 295 K) by in situ neutron diffraction analysis [110]. The deformation pathways for HEAs at ultralow temperatures were established. The interaction and competition between different deformation mechanisms were elucidated. As shown in Fig. 15, the serrated flow appears in the stress-strain curve at 15 K. The microstructure evolution after deformation is shown in Fig. 27. At room

temperature, a high density of dislocations piles up and the primary deformation mechanism is dislocation slip, as shown in Fig. 27(a). As shown in Fig. 27(b) and (c), there are a large number of stacking faults and very high-density twins which interact with each other to form a twin network at 15 K. The critical deformation stress corresponding to different mechanisms at 15 K by stacking fault probability (SFP) is shown in Fig. 28. The dotted line in Fig. 28 pinpoints the critical stress point of each deformation mechanism at 15 K: 1. Yield stress point ($\sigma_y \sim 718$ MPa); 2. Initial stress of stacking fault ($\sigma \sim 1075$ MPa); 3. Serrated flow initial stress ($\sigma \sim 1270$ MPa); 4. Massive serrations flow stress ($\sigma \sim 2000$ MPa). The origin of serrations at ultralow temperatures is attributed to the thermal instability or the mechanical instability of deformation. The heat

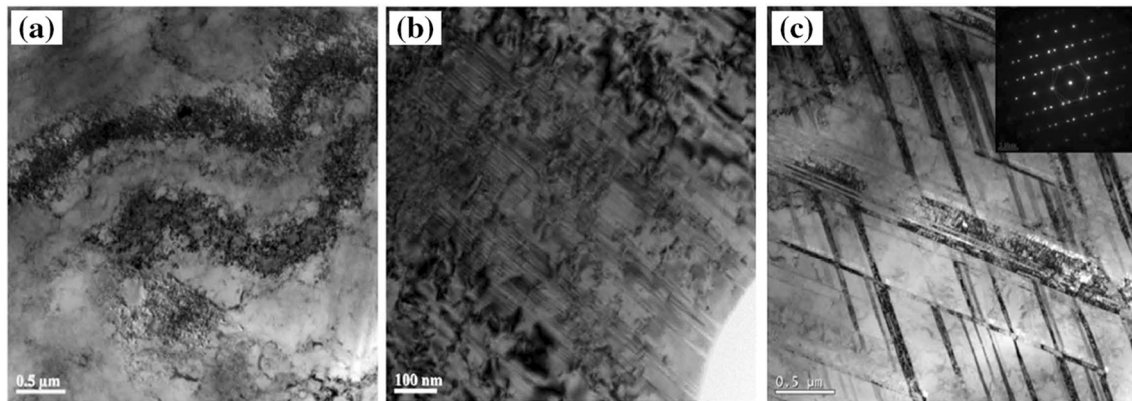


Figure 27 TEM images of fractured samples: **a** the dislocation pileups at room temperature, **b** large number of SFs and a very high density of closely spaced twins at 15 K, **c** intersecting

twinning network at 15 K [110]. Reproduced from [110] with permission from AAAS (Author: Muhammad Naeem).

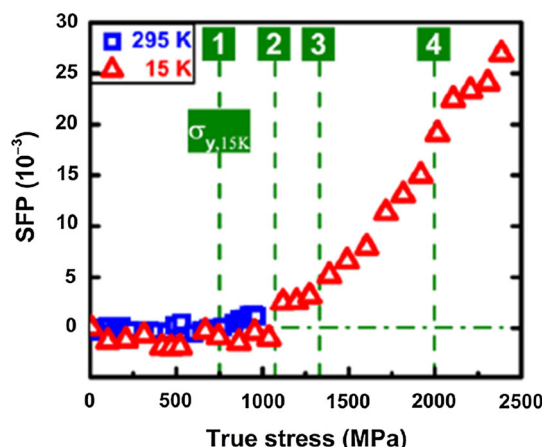


Figure 28 Deformation pathway of CrMnFeCoNi HEA at 15 K [110]. Reproduced from [110] with permission from AAAS (Author: Muhammad Naeem).

produced during deformation is not conducted away and causes localized heating and softening, which results in a stress drop. The pinning and pile-up of dislocations cause a very high stress concentration due to the mechanical instability of plastic deformation.

In summary, HEAs have a multi-component design concept, including high entropy, lattice distortion and sluggish diffusion effect. Lattice distortion and sluggish diffusion effect further induce solid solution strengthening. High mixing entropy promotes single-phase solid solution formation. HEAs with single-phase FCC solid solution have more intrinsic slip systems and lower SFE than those of pure metal and traditional FCC alloys. The schematic diagram of deformation behavior of HEAs is shown in Fig. 29. At low temperature, the dislocations

movement is inhibited and the SFE decreases. The complete $1/2 < 110 >$ -type dislocations are decomposed into $1/6 < 112 >$ Shockley partial dislocations and the twins or martensite phase are activated during deformation. The strengthening mechanisms are mainly twinning strengthening and phase transformation strengthening in addition to solid solution strengthening due to large lattice distortion and precipitation strengthening at low temperature. TWIP and TRIP hinder dislocation movement to delay necking fracture and increase the strain hardening rate, which improves the strength and plasticity of HEAs [11, 154, 155]. The unique complex chemistry and simple crystal structure of HEAs with low SFE are the key to the design of new materials for applications at low temperatures, where the multiple deformation mechanisms can be deployed in synergy to produce materials with high strength and superior ductility.

Conclusions

The HEAs have attracted extensive attention in the field of materials due to their unique composition since they were first defined in 2004. Researchers have been developing more systems of HEAs through alloy composition design. In addition to optimizing the composition, the properties and microstructure evolution of these alloys have been studied. It is found that HEAs exhibit excellent strength, plasticity and fracture toughness in the field of cryogenic temperature environment, which makes them have a potential application as low temperature

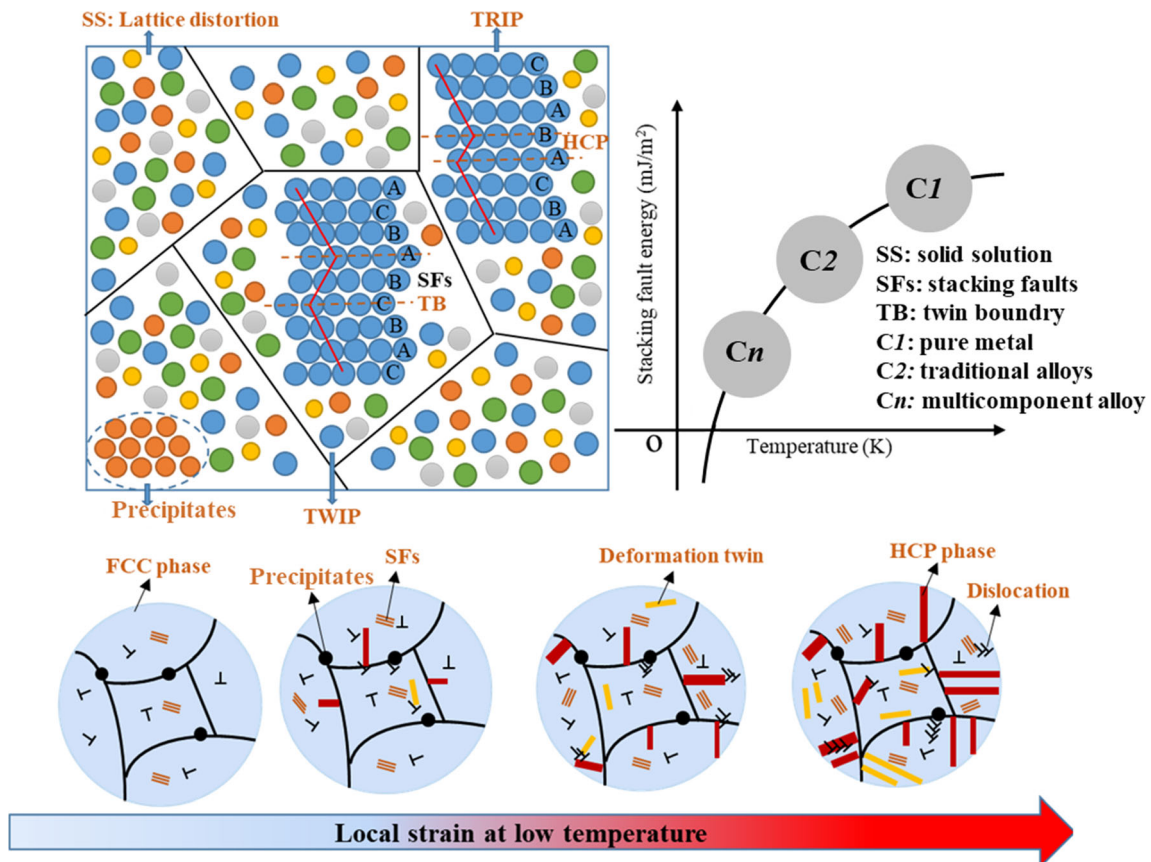


Figure 29 Schematic diagram of TWIP and TRIP strengthening mechanism, Shockley partial dislocation glide induced nucleation and growth of twins and martensitic phases.

structural materials in the future. Therefore, the research deformation mechanism and microstructure evolution of HEAs at low temperature provide a theoretical basis for the development and application of low-temperature structural materials. The low-temperature properties and deformation behavior of HEAs in this review are summarized as follows:

- (1) There are many factors affecting the properties of HEAs during low-temperature deformation, including phase structure, grain size, and SFE. The HEAs with FCC single-phase structure are the most widely studied materials to explore the low-temperature properties. They have more slip systems and are easier to deform at low temperature, which results in excellent plasticity. The hard second phase is also introduced into the single-phase alloy to form a multiphase structure. The stress is distributed to the hard and soft phases to improve the strength during low-temperature deformation.

BCC HEAs have a low strain hardening ability at low temperature.

- (2) The finer fragmented structure forms and the grains become smaller in the lamellar boundary and shear band. The yield strength of HEAs has a linear relationship with grain size at low temperature. HEAs are in good agreement with the Hall-Petch relationship at low temperatures, so the yield strength of the alloys can be improved by decreasing the grain size. The multi-component characteristics of HEAs have lower SFE at low temperature to increase the distance of two partial dislocations to form a stacking fault which benefits the deformation twinning and martensitic transformation.
- (3) HEAs have excellent mechanical properties and become one of the most damage-tolerant resistant materials at low temperature. At low temperature, the tensile strength and plasticity of HEAs are significantly improved compared with those at room temperature. The

compression strength of the alloys is obviously improved during low temperature deformation, but the plasticity is slightly decreased. The fracture toughness of HEAs is more than $200 \text{ MPa}\cdot\text{m}^{1/2}$, which is higher than that of most structural materials.

- (4) There are many kinds of deformation mechanisms in HEAs during low-temperature deformation, including dislocation slip, deformation twins, low-temperature phase transformation and serration flow. The coexistence of multiple deformation mechanisms of HEAs at low temperature has synergistic or competitive interaction.

Perspectives

In some special application environments, metallic materials must be exposed to extremely low temperatures, such as tanks, pressure vessels, pipelines in cold regions, fusion power structures, hydrocarbon exploration, and structural parts for aerospace applications. Therefore, the materials must have excellent low temperature mechanical properties, including strength, ductility and toughness, which is very important to ensure the structural integrity in low temperature service. It is found that HEAs have excellent mechanical properties (high strength, high plasticity and high fracture toughness) and have high damage resistance at low temperature. The synergistic or competitive effect of multiple deformation mechanisms provides new design ideas for the development and design of cryogenic materials. HEAs have great potential application as low temperature structural materials in the future. However, there are still many unsolved problems in the research on the deformation behavior of HEAs at low temperature.

- (1) The multi-component characteristics of HEAs lead to a complex atomic-scale structure. The lattice distortion, short-range order and stacking fault atomic-scale structures play an important role during low-temperature deformation. There are great difficulties in the characterization of complex atomic structures. It is necessary to establish quantitative models and realize atomic-scale characterization by detection methods. The atomic-scale models and

characterization of HEAs have been accurately established to better reveal the mechanism of deformation at low temperature.

- (2) The SFE of HEAs is closely dependent on composition and temperature. Low SFE is an important factor for the improvement of strength and ductility at low -temperature deformation. At present, the temperature-dependent behavior of SFE is predicted by simulations using first-principles methods. To validate the simulated results, a few studies have measured SFE of HEAs by experiment using TEM or XRD methods at room temperature. There is an obvious difference between the theoretical calculation and experimental calculation of SFE. Experimental methods cannot directly measure low-temperature SFE, as the dislocations or stacking faults of deformed samples at cryogenic temperature may change by preparation of samples at room temperature. It is necessary to develop new experimental methods and optimize the first-principles calculation method to measure low-temperature SFE. There is guidance for predicting low-temperature performance by establishing a logical correlation between the SFE and the deformation behavior.
- (3) HEAs overcome the strength–ductility trade-off of traditional alloys at low temperature, as the deformation mechanism transformation from dislocation at room temperature to deformation twins or martensitic at low temperature. The synergistic or competitive interaction of various deformation mechanisms at low temperature is still controversial. The critical stress activated by dislocation and twin and phase transformation mechanism needs to be studied in different high-entropy alloys to further reveal the law at low temperature. At extreme temperature, serration flow behavior is activated at critical stress. The origin of serrations at ultralow temperatures is attributed to the thermal instability or the mechanical instability of deformation. It is necessary to investigate the correlation between the thermal instability and mechanical instability.
- (4) At present, most studies focus on the properties of HEAs with single-phase FCC and precipitated strengthening FCC structures at low temperature. There is little research on the

low-temperature deformation behavior of HEAs with BCC and HCP structures. HEAs of various systems can be further studied at low temperature, which further reveals the low-temperature deformation mechanism by adjusting different phase structures. The different phase structure HEAs provide a wider range of structural design for application in extreme environments. The low-temperature research of HEAs is based on the theoretical research of small size samples. Large size samples with excellent mechanical properties will need to be studied at low temperature for future practical applications.

Acknowledgements

This work was supported by the National Outstanding Youth Science Fund Project of National Natural Science Foundation of China (No. 51825401) and the Postdoctoral Foundation of Heilongjiang Province (LBH-Z19154).

Declarations

Conflict of interest The authors declare that they have no known competing financial interests or personal relationships that could have appeared to influence the work reported in this paper.

References

- [1] Cantor B, Chang TH, Knight P, Vincent AJB (2004) Microstructural development in equiatomic multicomponent alloys. *Mater Sci Eng A* 375–377:213–218. <https://doi.org/10.1007/s10853-021-06111-w>
- [2] Yeh JW, Chen SK, Lin SJ, Gan JY, Chin TS, Shun TT, Tsau CH, Chang SY (2004) Nanostructured high-entropy alloys with multiple principal elements: novel alloy design concepts and outcomes. *Adv Eng Mater* 6:299–303. <https://doi.org/10.1002/adem.200300567>
- [3] Miracle DB, Senkov ON (2017) A critical review of high entropy alloys and related concepts. *Acta Mater* 122:448–511. <https://doi.org/10.1016/j.actamat.2016.08.081>
- [4] Gao MC, Yew JW, Zhang Y (2016) Design of High-Entropy Alloys. Springer, New York
- [5] Gludovatz B, Hohenwarter A, Thurston K, Bei HB, Wu ZG, George EP (2016) Exceptional damage-tolerance of a medium-entropy alloy CrCoNi at cryogenic temperatures. *Nat Commun* 7:10602. <https://doi.org/10.1038/ncomms10602>
- [6] Gludovatz B, Hohenwarter A, Catoor D (2014) A fracture-resistant high-entropy alloy for cryogenic applications. *Science* 345:1153–1158. <https://doi.org/10.1126/science.1254581>
- [7] Yong Z, Zuo TT, Zhi T, Gao MC, Dahmen KA, Liaw PK, Zhao PL (2014) Microstructures and properties of high-entropy alloys. *Prog Mater Sci* 61:1–93. <https://doi.org/10.1016/j.pmatsci.2013.10.001>
- [8] Shi PJ, Ren WL, Zheng TX, Xue ZM, Hou JC (2019) Enhanced strength-ductility synergy in ultrafine-grained eutectic high-entropy alloys by inheriting microstructural lamellae. *Nat Commun* 10:489. <https://doi.org/10.1038/s41467-019-08460-2>
- [9] Fu ZQ, Jiang L, Wardini JL, MacDonald BE, Wen HM, Xiong W, Zhang DL, Zhou YZ, Rupert TJ, Chen WP, Lavernia EJ (2018) A high-entropy alloy with hierarchical nanoprecipitates and ultrahigh strength. *Sci Adv* 4:8712. <https://doi.org/10.1126/sciadv.aat8712>
- [10] Zhang Z, Mao MM, Wang J, Gludovatz B, Zhang Z, Mao SX, George EP, Yu Q, Ritchie RO (2015) Nanoscale origins of the damage tolerance of the high-entropy alloy CrMnFeCoNi. *Nat Commun* 6:10143. <https://doi.org/10.1038/ncomms10143>
- [11] Li Z, Pradeep KG, Deng Y, Raabe D, Tasan CC (2016) Metastable high-entropy dual-phase alloys overcome the strength-ductility trade-off. *Nature* 534:227–230. <https://doi.org/10.1038/nature17981>
- [12] Senkov ON, Wilks GB, Scott JM, Miracle DB (2011) Mechanical properties of NbMoTaW and VNbMoTaW refractory high entropy alloys. *Intermetallics* 19:698–706. <https://doi.org/10.1016/j.intermet.2011.01.004>
- [13] Tsai MH, Hao Y, Cheng G, Xu W, Jian WW, Chuang MH, Juan CC, Yeh AC, Lin SJ, Zhu Y (2013) Significant hardening due to the formation of a sigma phase matrix in a high entropy alloy. *Intermetallics* 33:81–86. <https://doi.org/10.1016/j.intermet.2012.09.022>
- [14] Juan CC, Hsu CY, Tsai CW, Wang WR, Sheu TS, Yeh JW, Chen SK (2013) On microstructure and mechanical performance of AlCoCrFeMo_{0.5}Ni_x high-entropy alloys. *Intermetallics* 32:401–407. <https://doi.org/10.1016/j.intermet.2012.09.008>
- [15] Varma SK, Sanchez F, Ramana CV (2020) Microstructures in a Nb-Cr-V-W-Ta high entropy alloy during annealing. *J Mater Sci Technol* 53:66–72. <https://doi.org/10.1016/j.jmst.2020.03.028>

- [16] Lu C, Niu L, Chen N, Jin K, Yang T, Xiu P, Zhang Y, Gao F, Bei H, Shi S (2016) Enhancing radiation tolerance by controlling defect mobility and migration pathways in multicomponent single-phase alloys. *Nat Commun* 7:13564. <https://doi.org/10.1038/ncomms13564>
- [17] Pogrebnyak AD, Yakushchenko IV, Bondar OV, Beresnev VM, Kozak C (2016) Irradiation resistance, microstructure and mechanical properties of nanostructured (TiZrHfVNb-Ta)N coatings. *J Alloy Compd* 679:155–163. <https://doi.org/10.1016/j.jallcom.2016.04.064>
- [18] Huang X, Miao J, Luo AA (2018) Lightweight AlCrTiV high-entropy alloys with dual-phase microstructure via microalloying. *J Mater Sci* 54:2271. <https://doi.org/10.1007/s10853-018-2970-4>
- [19] Zhang C, Zhang F, Diao H, Gao MC, Tang Z, Poplawsky JD, Liaw PK (2016) Understanding phase stability of Al-Co-Cr-Fe-Ni high entropy alloys. *Mater Des* 109:425–433. <https://doi.org/10.1016/j.matdes.2016.07.073>
- [20] Zhang Y, Zhou YJ, Lin JP, Chen GL, Liaw PK (2008) Solid-solution phase formation rules for multi-component alloys. *Adv Eng Mater* 10:534–538. <https://doi.org/10.1002/adem.200700240>
- [21] Zhang Y, Lu ZP, Ma SG, Liaw PK, Tang Z, Cheng YQ, Gao MC (2014) Guidelines in predicting phase formation of high-entropy alloys. *MRS Commun* 4:57–62. <https://doi.org/10.1557/mrc.2014.11>
- [22] Chen P, Li S, Zhou Y, Yan M, Attallah MM (2020) Fabricating CoCrFeMnNi high entropy alloy via selective laser melting in-situ alloying. *J Mater Sci Technol* 43:40–43. <https://doi.org/10.1016/j.jmst.2020.01.002>
- [23] Wang AG, An XH, Gu J, Wang XG, Li LL, Li WL, Song M, Duan QQ, Zhang ZF, Liao XZ (2020) Effect of grain size on fatigue cracking at twin boundaries in a CoCr-FeMnNi high-entropy alloy. *J Mater Sci Technol* 39:1–6
- [24] Zhang KB, Fu ZY, Zhang JY, Shi J, Wang WM, Wang H, Wang YC, Zhang QJ (2010) Annealing on the structure and properties evolution of the CoCrFeNiCuAl high-entropy alloy. *J Alloy Compd* 502:295–299. <https://doi.org/10.1016/j.jallcom.2009.11.104>
- [25] Lin CM, Tsai HL, Bor HY (2010) Effect of aging treatment on microstructure and properties of high-entropy Cu_{0.5}-CoCrFeNi alloy. *Intermetallics* 18:1244–1250. <https://doi.org/10.1016/j.intermet.2010.03.030>
- [26] Niu S, Kou H, Tong G, Yu Z, Wang J, Li J (2016) Strengthening of nanoprecipitations in an annealed Al_{0.5}-CoCrFeNi high entropy alloy. *Mater Sci Eng A* 671:82–86. <https://doi.org/10.1016/j.msea.2016.06.040>
- [27] Jang MJ, Praveen S, Sung HJ, Bae J (2018) High-temperature tensile deformation behavior of hot rolled CrMnFeCoNi high-entropy alloy. *J Alloy Compd* 730:242–248. <https://doi.org/10.1016/j.jallcom.2017.09.293>
- [28] Qin G, Chen R, Liaw PK, Gao Y, Wang L, Su Y, Ding H, Guo J, Li X (2020) An as-cast high-entropy alloy with remarkable mechanical properties strengthened by nanometer precipitates. *Nanoscale* 12:3965–3976. <https://doi.org/10.1039/C9NR08338C>
- [29] Hu GW, Zeng LC, Du H, Liu XW, Wu Y, Gong P, Fan ZT, Hu Q, George EP (2020) Tailoring grain growth and solid solution strengthening of single-phase CrCoNi medium-entropy alloys by solute selection. *J Mater Sci Technol* 54:196–205. <https://doi.org/10.1016/j.jmst.2020.02.073>
- [30] Bhattacharjee T, Wani IS, Sheikh S, Clark IT, Okawa T, Guo S, Bhattacharjee PP, Tsuji N (2018) Simultaneous strength-ductility enhancement of a nano-lamellar AlCoCrFeNi_{2.1} eutectic high entropy alloy by cryo-rolling and annealing. *Sci Rep* 8:3276
- [31] Sathiaraj GD, Bhattacharjee PP, Tsai CW, Yeh JW (2016) Effect of heavy cryo-rolling on the evolution of microstructure and texture during annealing of equiatomic CoCrFeMnNi high entropy alloy. *Intermetallics* 69:1–9. <https://doi.org/10.1016/j.intermet.2015.10.005>
- [32] Zhou YJ, Zhang Y, Wang YL, Chen GL (2007) Solid solution alloys of AlCoCrFeNiTi_x with excellent room-temperature mechanical properties. *Appl Phys Lett* 90:181904. <https://doi.org/10.1063/1.2734517>
- [33] Tong CJ, Chen YL, Yeh JW, Lin SJ, Chen SK, Shun TT, Tsau CH, Chang SY (2005) Microstructure characterization of Al_xCoCrCuFeNi high-entropy alloy system with multi-principal elements. *Metall Mater Trans A* 36:881–893. <https://doi.org/10.1007/s11661-005-0283-0>
- [34] Zhou YJ, Zhang Y, Wang YL, Chen GL (2007) Microstructure and compressive properties of multicomponent Al_xTiVCrMnFeCoNiCu_{100-x} high-entropy alloys. *Mater Sci Eng A* 454–455:260–265. <https://doi.org/10.1016/j.msea.2006.11.049>
- [35] Fazakas É, Zadorozhny V, Louzguine-Luzgin DV (2015) Effect of iron content on the structure and mechanical properties of Al₂₅Ti₂₅Ni₂₅Cu₂₅ and (AlTi)_{60-x}Ni₂₀Cu₂₀Fe_x ($x=15, 20$) high-entropy alloys. *Appl Surf Sci* 358:549–555. <https://doi.org/10.1016/j.apsusc.2015.07.207>
- [36] Tong CJ, Chen MR, Chen SK et al (2005) Mechanical performance of the Al_xCoCrCuFeNi high-entropy alloy system with multiprincipal elements. *Metall Mater Trans A* 36A:1263–1271. <https://doi.org/10.1007/s11661-005-0218-9>
- [37] Wang XF, Zhang Y, Qiao Y, Chen GL (2007) Novel microstructure and properties of multicomponent CoCrCuFeNiTi_x alloys. *Intermetallics* 15:357–362. <https://doi.org/10.1007/s11661-005-0218-9>

- [38] Li D, Zhang Y (2016) The ultrahigh charpy impact toughness of forged $\text{Al}_x\text{CoCrFeNi}$ high entropy alloys at room and cryogenic temperatures. *Intermetallics* 70:24–28. <https://doi.org/10.1016/j.intermet.2015.11.002>
- [39] Gali A, George EP (2013) Tensile properties of high-and medium-entropy alloys. *Intermetallics* 39:74–78. <https://doi.org/10.1016/j.intermet.2013.03.018>
- [40] Otto F, Dlouhý A, Somsen C, Bei H, Eggeler G, George EP (2013) The influences of temperature and microstructure on the tensile properties of a CoCrFeMnNi high-entropy alloy. *Acta Mater* 61:5743–5755. <https://doi.org/10.1016/j.actamat.2013.06.018>
- [41] Jo YH, Jung S, Choi WM, Sohn SS, Kim HS, Lee BJ, Kim NJ, Lee S (2017) Cryogenic strength improvement by utilizing room-temperature deformation twinning in a partially recrystallized VCrMnFeCoNi high-entropy alloy. *Nat Commun* 8:15719. <https://doi.org/10.1038/ncomms15719>
- [42] Zhang DD, Zhang JY, Kuang J, Liu G, Sun J (2021) Superior strength-ductility synergy and strain hardenability of Al/Ta co-doped NiCoCr twinned medium-entropy alloy for cryogenic applications. *Acta Mater* 220:117288. <https://doi.org/10.1016/j.actamat.2021.117288>
- [43] Moon J, Tabachnikova E, Shumilin S, Hryhorova T, Estrin Y, Brechtl J, Liaw PK, Wang W, Dahmen KA, Zargaran A, Do BJW, HS, Lee BJ, Kim HS, (2021) Deformation behavior of a Co-Cr-Fe-Ni-Mo medium-entropy alloy at extremely low temperatures. *Mater Today* 50:55–68. <https://doi.org/10.1016/j.mattod.2021.08.001>
- [44] Moon J, Bouaziz O, Kim HS, Estrin Y (2021) Twinning engineering of a CoCrFeMnNi high-entropy alloy. *Scr Mater* 197:113808. <https://doi.org/10.1016/j.scriptamat.2021.113808>
- [45] He Z, Jia N, Wang H, Yan H, Shen Y (2021) Synergy effect of multi-strengthening mechanisms in FeMnCoCrN HEA at cryogenic temperature. *J Mater Sci Technol* 86:158–170. <https://doi.org/10.1016/j.jmst.2020.12.079>
- [46] Haftlang F, Asghari-Rad P, Moon J, Zargaran A, Lee KA, Hong SJ, Kim HS (2021) Simultaneous effects of deformation-induced plasticity and precipitation hardening in metastable non-equiautomic FeNiCoMnTiSi ferrous medium-entropy alloy at room and liquid nitrogen temperatures. *Scr Mater* 202:114013. <https://doi.org/10.1016/j.scriptamat.2021.114013>
- [47] Tang L, Yan K, Cai B, Wang Y, Liu B, Kabra S, Attallah MM, Liu Y (2020) Deformation mechanisms of $\text{FeCoCrNiMo}_{0.2}$ high entropy alloy at 77 and 15 K. *Scr Mater* 178:166–170. <https://doi.org/10.1016/j.scriptamat.2019.11.026>
- [48] Seol JB, Bae JW, Kim JG, Sung H, Li Z, Lee HH, Shim SH, Jang JH, Ko WS, Hong SI, Kim HS (2020) Short-range order strengthening in boron-doped high-entropy alloys for cryogenic applications. *Acta Mater* 194:366–377. <https://doi.org/10.1016/j.actamat.2020.04.052>
- [49] Li Q, Zhang TW, Qiao JW, Ma SG, Zhao D, Lu P, Wang ZH (2020) Mechanical properties and deformation behavior of dual-phase Al06CoCrFeNi high-entropy alloys with heterogeneous structure at room and cryogenic temperatures. *J Alloy Compd* 816:152663. <https://doi.org/10.1016/j.jallcom.2019.152663>
- [50] Kwon H, Moon J, Bae JW, Park JM, Son S, Do HS, Lee BJ, Kim HS (2020) Precipitation-driven metastability engineering of carbon-doped CoCrFeNiMo medium-entropy alloys at cryogenic temperature. *Scr Mater* 188:140–145. <https://doi.org/10.1016/j.scriptamat.2020.07.023>
- [51] Rao K, Yu W, Ritchie RO (1989) Cryogenic toughness of commercial aluminum-lithium alloys: role of delamination toughening. *Metall Mater Trans A* 20:485–497. <https://doi.org/10.1007/bf02653929>
- [52] Martin S, Wolf S, Martin U, Krüger L, Rafaja D (2014) Deformation mechanisms in austenitic TRIP/TWIP steel as a function of temperature. *Metall Mater Trans A* 47:49–58. <https://doi.org/10.1007/s11661-014-2684-4>
- [53] Tan Y, Chen RR, Fang H, Liu Y, Cui H, Su Y, Guo J, Fu H (2022) Enhanced strength and ductility in Ti46Al4Nb1Mo alloys via boron addition. *J Mater Sci Technol* 102:16–23. <https://doi.org/10.1016/j.jmst.2021.06.037>
- [54] Otto F, Dlouhý A, Pradeep KG, Kuběnová M, Raabe D, Eggeler G, George EP (2016) Decomposition of the single-phase high-entropy alloy CrMnFeCoNi after prolonged anneals at intermediate temperatures. *Acta Mater* 112:40–52. <https://doi.org/10.1016/j.actamat.2016.04.005>
- [55] Aizenshtein M, Strumza E, Brosh E, Hayun S (2020) Precipitation kinetics, microstructure and equilibrium state of A2 and B2 phases in multicomponent $\text{Al}_{2.75}\text{CoCrFeNi}$ alloy. *J Mater Sci* 55:7016–7028. <https://doi.org/10.1007/s10853-020-04487-9>
- [56] Qiao JW, Ma SG, Huang EW, Chuang CP, Liaw PK, Zhang Y (2011) Microstructural characteristics and mechanical behaviors of AlCoCrFeNi high-entropy alloys at ambient and cryogenic temperatures. *Mater Sci Forum* 688:419–425. <https://doi.org/10.4028/www.scientific.net/msf.688.419>
- [57] Eleti RR, Stepanov N, Zherebtsov S (2020) Mechanical behavior and thermal activation analysis of HfNbTaTiZr body-centered cubic high-entropy alloy during tensile deformation at 77 K. *Scr Mater* 188:118–123. <https://doi.org/10.1016/j.scriptamat.2020.07.028>
- [58] Senkov ON, Wilks GB, Miracle DB, Chuang CP, Liaw PK (2010) Refractory high-entropy alloys. *Intermetallics*

- 18:1758–1765. <https://doi.org/10.1016/j.intermet.2010.05.014>
- [59] Yao MJ, Pradeep KG, Tasan CC, Raabe D (2014) A novel, single phase, non-equiautomic FeMnNiCoCr high-entropy alloy with exceptional phase stability and tensile ductility. *Scr Mater* 72–73:5–8. <https://doi.org/10.1016/j.scriptamat.2013.09.030>
- [60] Li D, Li C, Feng T, Zhang Y, Sha G, Lewandowski JJ, Liaw PK, Zhang Y (2017) High-entropy $\text{Al}_{0.3}\text{CoCrFeNi}$ alloy fibers with high tensile strength and ductility at ambient and cryogenic temperatures. *Acta Mater* 123:285–294. <https://doi.org/10.1016/j.actamat.2016.10.038>
- [61] Liu WH, Lu ZP, He JY, Luan JH, Wang ZJ, Liu B, Liu Y, Chen MW, Liu CT (2016) Ductile CoCrFeNiMo_x high entropy alloys strengthened by hard intermetallic phases. *Acta Mater* 116:332–342. <https://doi.org/10.1016/j.actamat.2016.06.063>
- [62] Lu Y, Gao X, Jiang L, Chen Z, Wang T, Jie J, Kang H, Zhang Y, Guo S, Ruan H, Zhao Y, Cao Z, Li T (2017) Directly cast bulk eutectic and near-eutectic high entropy alloys with balanced strength and ductility in a wide temperature range. *Acta Mater* 124:143–150. <https://doi.org/10.1016/j.actamat.2016.11.016>
- [63] Shi P, Ren W, Zheng T, Ren Z, Hou X, Peng J, Hu P, Gao Y, Zhong Y, Liaw PK (2019) Enhanced strength-ductility synergy in ultrafine-grained eutectic high-entropy alloys by inheriting microstructural lamellae. *Nat Commun* 10:489. <https://doi.org/10.1038/s41467-019-08460-2>
- [64] Bhattacharjee T, Zheng R, Chong Y, Sheikh S, Guo S, Clark IT, Okawa T, Wani IS, Bhattacharjee PP, Shibata A, Tsuji N (2018) Effect of low temperature on tensile properties of AlCoCrFeNi_{2.1} eutectic high entropy alloy. *Mater Chem Phys* 210:207–212. <https://doi.org/10.1016/j.matchemphys.2017.06.023>
- [65] Park JM, Moon J, Bae JW, Kim DH, Jo YH, Lee S, Kim HS (2019) Role of BCC phase on tensile behavior of dual-phase $\text{Al}_{0.5}\text{CoCrFeMnNi}$ high-entropy alloy at cryogenic temperature. *Mater Sci Eng A* 746:443–447. <https://doi.org/10.1016/j.msea.2019.01.041>
- [66] Jo YH, Choi WM, Kim DG, Zargaran A, Lee K, Sung H, Sohn SS, Kim HS, Lee BJ, Lee S (2019) Utilization of brittle σ phase for strengthening and strain hardening in ductile VCrFeNi high-entropy alloy. *Mater Sci Eng A* 743:665–674. <https://doi.org/10.1016/j.msea.2018.11.136>
- [67] Nayan N, Singh G, Murty SVSN, Jha MAK, B, Pant KM, George U, (2014) Hot deformation behaviour and microstructure control in AlCrCuNiFeCo high entropy alloy. *Intermetallics* 55:145–153. <https://doi.org/10.1016/j.intermet.2014.07.019>
- [68] Kao YF, Chen TJ, Chen SK, Yeh JW (2009) Microstructure and mechanical property of as-cast, homogenized and -deformed $\text{Al}_x\text{CoCrFeNi}$ ($0 \leq x \leq 2$) high-entropy alloys. *J Alloy Compd* 488:57–64. <https://doi.org/10.1016/j.jallcom.2009.08.090>
- [69] Tsai CW, Chen YL, Tsai MH, Yeh JW, Shun TT, Chen SK (2009) Deformation and annealing behaviors of high-entropy alloy $\text{Al}_{0.5}\text{CoCrCuFeNi}$. *J Alloy Compd* 486:427–435. <https://doi.org/10.1016/j.jallcom.2009.06.182>
- [70] Kuznetsov AV, Shaysultanov DG, Stepanov ND, Salishchev G, Senkov ON (2012) Tensile properties of an AlCrCuNiFeCo high-entropy alloy in as-cast and wrought conditions. *Mater Sci Eng A* 533:107–118. <https://doi.org/10.1016/j.msea.2011.11.045>
- [71] Shaysultanov DG, Stepanov ND, Kuznetsov AV, Salishchev GA, Senkov ON (2013) Phase composition and superplastic behavior of a wrought AlCoCrCuFeNi high-entropy alloy. *JOM* 65:1815–1828. <https://doi.org/10.1007/s11837-013-0754-5>
- [72] Stepanov N, Tikhonovsky M, Yurchenko N, Zyabkin D, Salishchev G (2015) Effect of cryo-deformation on structure and properties of CoCrFeNiMn high-entropy alloy. *Intermetallics* 59:8–17. <https://doi.org/10.1016/j.intermet.2014.12.004>
- [73] Liu WH, Wu Y, He JY, Nieh TG, Lu ZP (2013) Grain growth and the Hall-Petch relationship in a high-entropy FeCrNiCoMn alloy. *Scr Mater* 68:526–529. <https://doi.org/10.1016/j.scriptamat.2012.12.002>
- [74] Sun S, Tian Y, Lin HR, Dong XG, Zhang Z (2019) Temperature dependence of the Hall-Petch relationship in CoCrFeMnNi high-entropy alloy. *J Alloy Compd* 806:992–998. <https://doi.org/10.1016/j.jallcom.2019.07.357>
- [75] Lei Z, Liu X, Wu Y, Wang H, Jiang S, Wang S HX, Wu Y, Gault B, Kontis P, Raabe D, Gu L, Zhang Q, Chen H, Wang H, Liu J, An K, Zeng Q, Nieh TG, Lu Z (2018) Enhanced strength and ductility in a high-entropy alloy via ordered oxygen complexes. *Nature* 563:546–550. <https://doi.org/10.1038/s41586-018-0685-y>
- [76] Asadiya M, Yang SG, Zhang YF, Lemay C, Apelian D, Zhong Y (2021) A review of the design of high-entropy aluminum alloys: a pathway for novel Al alloys. *J Mater Sci* 56:12093–12110. <https://doi.org/10.1007/s10853-021-06042-6>
- [77] Zhang F, Wu Y, Lou H, Zeng Z, Prakapenka VB, Greenberg E, Ren Y, Yan J, Okasinski JS, Liu X, Liu Y, Zeng Q, Lu Z (2017) Polymorphism in a high-entropy alloy. *Nat Commun* 8:15687. <https://doi.org/10.1038/ncomms15687>

- [78] Park KT, Jin KG, Han SH, Hwang SW, Choi K, Lee CS (2010) Stacking fault energy and plastic deformation of fully austenitic high manganese steels: effect of Al addition. *Mater Sci Eng A* 527:3651–3661. <https://doi.org/10.1016/j.msea.2010.02.058>
- [79] Kim J, Lee SJ, De Cooman BC (2011) Effect of Al on the stacking fault energy of Fe-18Mn-0.6C twinning-induced plasticity. *Scr Mater* 65:363–366. <https://doi.org/10.1016/j.scriptamat.2011.05.014>
- [80] Huang S, Li Wei LuS, Tian FY, Tian J, Holmström E, Vitos L (2015) Temperature dependent stacking fault energy of FeCrCoNiMn high entropy alloy. *Scr Mater* 108:44–47. <https://doi.org/10.1016/j.scriptamat.2015.05.041>
- [81] Dumay A, Chateau JP, Allain S, Migot S, Bouaziz O (2008) Influence of addition elements on the stacking-fault energy and mechanical properties of an austenitic Fe-Mn-C steel. *Mater Sci Eng A* 483–484:184–187. <https://doi.org/10.1016/j.msea.2008.12.170>
- [82] Frommeyer G, Brüx U, Neumann P (2003) Supra ductile and high-strength manganese-TRIP/TWIP steels for high energy absorption purposes. *ISIJ Int* 43:438–446. <https://doi.org/10.2355/isijinternational.43.438>
- [83] Martin S, Wolf S, Martin U et al (2016) Deformation mechanisms in austenitic TRIP/TWIP steel as a function of temperature. *Metall Mater Trans A* 47:49–58. <https://doi.org/10.1007/s11661-014-2684-4>
- [84] Huang S, Li W, Lu S, Krüger L, Rafaja D (2015) Temperature dependent stacking fault energy of FeCrCoNiMn high entropy alloy. *Scr Mater* 108:44–47. <https://doi.org/10.1016/j.scriptamat.2015.05.041>
- [85] Zunger A, Wei S, Ferreira LG, Bernard JE (1990) Special quasirandom structures. *Phys Rev Lett* 65:353–356. <http://doi.org/10.1103/PhysRevLett.65.353>
- [86] Qiu S, Zhang XC, Zhou J, Cao S, Yu H, Hu QM, Sun Z (2020) Influence of lattice distortion on stacking fault energies of CoCrFeNi and Al-CoCrFeNi high entropy alloys. *J Alloy Compd* 846:156321. <https://doi.org/10.1016/j.jallcom.2020.156321>
- [87] Huang X, Miao J, Li S, Taylor CD, Luo AA (2021) Co-free CuFeMnNi high-entropy alloy with tunable tensile properties by thermomechanical processing. *J Mater Sci* 56:7670–7680. <https://doi.org/10.1007/s10853-020-05686-0>
- [88] Liu SF, Wu Y, Wang HT, He JY, Liu JB, Chen CX, Liu XJ, Wang H, Lu ZP (2018) Stacking fault energy of face-centered-cubic high entropy alloys. *Intermetallics* 93:269–273. <https://doi.org/10.1016/j.intermet.2017.10.004>
- [89] Tian X, Zhang Y (2009) Effect of Si content on the stacking fault energy in γ -Fe–Mn–Si–C alloys: part I. X-ray diffraction line profile analysis. *Mater Sci Eng A* 516:73–77. <https://doi.org/10.1016/j.msea.2009.02.031>
- [90] Zaddach AJ, Niu C, Koch CC, Irving DL (2013) Mechanical properties and stacking fault energies of NiFeCrCoMn high-entropy alloy. *JOM* 65:1780–1789. <https://doi.org/10.1007/s11837-013-0771-4>
- [91] Jeong K, Jin JE, Jung YS, Kang S, Lee YK (2013) The effects of Si on the mechanical twinning and strain hardening of Fe-18Mn-0.6C twinning-induced plasticity steel. *Acta Mater* 61:3399–3419. <https://doi.org/10.1016/j.actamat.2013.02.031>
- [92] Huang S, Wu H, Zhu H, Xie Z (2021) Effect of niobium addition upon microstructure and tensile properties of CrMnFeCoNix high entropy alloys. *Mater Sci Eng A* 809:140959. <https://doi.org/10.1016/j.msea.2021.140959>
- [93] Cecil GR, Anthony WT (1977) The composition dependence of stacking fault energy in austenitic stainless steels. *Metall Mater Trans A* 8:1901–1906. <https://doi.org/10.1007/bf02646563>
- [94] Raymond ES, Richard PR (1976) Stacking fault energies of fcc fe-Ni alloys by x-ray diffraction line profile analysis. *Metall Mater Trans A* 7:359–363. <https://doi.org/10.1007/bf02642831>
- [95] Ding J, Yu Q, Asta M, Ritchie RO (2018) Tunable stacking fault energies by tailoring local chemical order in CrCoNi medium-entropy alloys. *Proc Natl Acad Sci* 115:8919. <https://doi.org/10.1073/pnas.1808660115>
- [96] Niu C, LaRosa CR, Miao J, Mills MJ, Ghazisaeidi M (2018) Magnetically-driven phase transformation strengthening in high entropy alloys. *Nat Commun* 9:1363. <https://doi.org/10.1038/s41467-018-03846-0>
- [97] Laplanche G, Kostka A, Reinhart C, Hunfeld J, Eggeler G, George EP (2017) Reasons for the superior mechanical properties of medium-entropy CrCoNi compared to high-entropy CrMnFeCoNi. *Acta Mater* 128:292–303. <https://doi.org/10.1016/j.actamat.2017.02.036>
- [98] Wang Y, Liu B, Yan K, Wang M, Kabra S, Chiu YL, Dye D, Lee PD, Liu Y, Cai B (2018) Probing deformation mechanisms of a FeCoCrNi high-entropy alloy at 293 and 77 K using in situ neutron diffraction. *Acta Mater* 154:79–89. <https://doi.org/10.1016/j.actamat.2018.05.013>
- [99] Woo W, Naeem M, Jeong JS, Lee CM, Harjo S, Kawasaki T, He H, Wang XL (2020) Comparison of dislocation density, twin fault probability, and stacking fault energy between CrCoNi and CrCoNiFe medium entropy alloys deformed at 293 and 140K. *Mater Sci Eng A* 781:139224. <https://doi.org/10.1016/j.msea.2020.139224>
- [100] George EP, Curtin WA, Tasan CC (2020) High entropy alloys: A focused review of mechanical properties and

- deformation mechanisms. *Acta Mater* 188:435–474. <http://doi.org/10.1016/j.actamat.2019.12.015>
- [101] Okamoto NL, Fujimoto S, Kambara Y, Kawamura M, Chen ZM, Matsunoshita H, Tanaka K, Inui H, George EP (2016) Size effect, critical resolved shear stress, stacking fault energy and solid solution strengthening in the CrMnFe-CoNi high-entropy alloy. *Sci Rep* 6:35863. <https://doi.org/10.1038/srep35863>
- [102] Chandan AK, Tripathy S, Sen B, Ghosh M, Ghosh-Chowdhury S (2021) Temperature dependent deformation behavior and stacking fault energy of Fe₄₀Mn₄₀Co₁₀Cr₁₀ alloy. *Scr Mater* 199:113891. <https://doi.org/10.1016/j.scriptamat.2021.113891>
- [103] Liu SF, Wu Y, Wang HT, Lin WT, Shang YY, Liu JB, An K, Liu XJ, Wang H, Lu ZP (2019) Transformation-reinforced high-entropy alloys with superior mechanical properties via tailoring stacking fault energy. *J Alloy Compd* 792:444–455. <https://doi.org/10.1016/j.jallcom.2019.04.035>
- [104] Liu J, Chen C, Xu Y, Wu S, Wang G, Wang H, Fang Y, Meng L (2017) Deformation twinning behaviors of the low stacking fault energy high-entropy alloy: An in-situ TEM study. *Scr Mater* 137:9–12. <https://doi.org/10.1016/j.scriptamat.2017.05.001>
- [105] Sun X, Zhang H, Li W, Ding X, Wang Y, Vitos L (2019) Generalized stacking fault energy of Al-doped CrMnFe-CoNi high-entropy alloy. *Nanomaterials* 10:59. <https://doi.org/10.3390/nano10010059>
- [106] De-Cooman BC, Estrin Y, Kim SK (2018) Twinning-induced plasticity (TWIP) steels. *Acta Mater* 142:283–362. <https://doi.org/10.1016/j.actamat.2017.06.046>
- [107] Sohn SS, Hong S, Lee J, Suh BC, Kim SK, Lee BJ, Kim NJ, Lee S (2015) Effects of Mn and Al contents on cryogenic-temperature tensile and Charpy impact properties in four austenitic high-Mn steels. *Acta Mater* 100:39–52. <https://doi.org/10.1016/j.actamat.2015.08.027>
- [108] Ritchie RO, Knott JF, Rice JR (1973) On the relationship between critical tensile stress and fracture toughness in mild steel. *J Mech Phys Sol* 21(6):395–410. [https://doi.org/10.1016/0022-5096\(73\)90008-2](https://doi.org/10.1016/0022-5096(73)90008-2)
- [109] Yang F, Dong L, Cai L, Hu X, Fang F (2021) Mechanical properties of FeMnCoCr high entropy alloy alloyed with C/Si at low temperatures. *J Alloy Compd* 859:157876. <https://doi.org/10.1016/j.jallcom.2020.157876>
- [110] Naeem M, He H, Zhang F, Huang H, Harjo S, Kawasaki T, Wang B, Lan S, Wu Z, Wang F, Wu Y, Lu Z, Zhang Z, Liu CT, Wang XL (2020) Cooperative deformation in high-entropy alloys at ultralow temperatures. *Sci Adv* 6:2375–2548. <https://doi.org/10.1126/sciadv.aax4002>
- [111] Naeem M, He H, Harjo S, Kawasaki T, Lin W, Kai JJ, Wu Z, Lan S, Wang XL (2021) Temperature-dependent hardening contributions in CrFeCoNi high-entropy alloy. *Acta Mater* 221:117371. <https://doi.org/10.1016/j.actamat.2021.117371>
- [112] Ding Q, Zhang Y, Chen X, Fu X, Chen D, Chen S, Gu L, Wei F, Bei H, Gao Y, Wen M, Li J, Zhang Z, Zhu T, Ritchie RO, Yu Q (2019) Tuning element distribution, structure and properties by composition in high-entropy alloys. *Nature* 574:223. <https://doi.org/10.1038/s41586-019-1617-1>
- [113] Wu Z, Bei H, Pharr GM, George EP (2014) Temperature dependence of the mechanical properties of equiatomic solid solution alloys with face-centered cubic crystal structures. *Acta Mater* 81:428–441. <https://doi.org/10.1016/j.actamat.2014.08.026>
- [114] Jang MJ, Kwak H, Lee YW, Jeong Y, Choi J, Jo YH, Choi WM, Sung HJ, Yoon EY, Praveen S (2019) Plastic deformation behavior of 40Fe-25Ni-15Cr-10Co-10V high-entropy alloy for cryogenic applications. *Met Mater Int* 25:277–284. <https://doi.org/10.1007/s12540-018-0184-6>
- [115] Li Q, Zhang TW, Qiao JW, Ma SG, Zhao D, Lu P, Xu B, Wang ZH (2019) Superior tensile properties of Al03 CoCrFeNi high entropy alloys with B2 precipitated phases at room and cryogenic temperatures. *Mater Sci Eng A* 767:138424. <https://doi.org/10.1016/j.msea.2019.138424>
- [116] Xia S, Zhang Y (2018) Deformation mechanisms of Al_{0.1}CoCrFeNi high entropy alloy at ambient and cryogenic temperatures. *Mater Sci Eng A* 733:408–413. <https://doi.org/10.1016/j.msea.2018.07.073>
- [117] Tsai CW, Tsai MH, Yeh JW, Yang CC (2010) Effect of temperature on mechanical properties of Al_{0.5}CoCrCuFeNi wrought alloy. *J Alloy Compd* 490:160–165. <https://doi.org/10.1016/j.jallcom.2009.10.088>
- [118] Laktionova MA, Tabchnikova ED, Tang Z, Liaw PK (2013) Mechanical properties of the high-entropy alloy Ag_{0.5}CoCrCuFeNi at temperatures of 4.2–300K. *Low Temp Phys* 39(7):630–632. <https://doi.org/10.1063/1.4813688>
- [119] Tabachnikova ED, Podolskiy AV, Laktionova MO, Bereznaja NA, Tikhonovsky MA, Tortika AS (2017) Mechanical properties of the CoCrFeNiMnVx high entropy alloys in temperature range 4.2–300 K. *J Alloy Compd* 698:501–509. <https://doi.org/10.1016/j.jallcom.2016.12.154>
- [120] Wang Y, Ma E (2004) On the origin of ultrahigh cryogenic strength of nanocrystalline metals. *Appl Phys Lett* 85:2750–2752. <https://doi.org/10.1063/1.1799238>
- [121] Guo X, Xie X, Ren J, Laktionova M, Tabachnikova E, Yu L, Cheung WS, Dahmen KA, Liaw PK (2017) Plastic dynamics of the Al_{0.5}CoCrCuFeNi high entropy alloy at

- cryogenic temperatures: Jerky flow, stair-like fluctuation scaling behavior and non-chaotic state. *Appl Phys Lett* 111(25):251905. <https://doi.org/10.1063/1.5004241>
- [122] Jo YH, Doh KY, Kim DG, Lee K, Kim DW, Sung H, Sohn SS, Lee D, Kim HS, Lee BJ, Lee S (2019) Cryogenic-temperature fracture toughness analysis of non-equia-atomic V₁₀Cr₁₀Fe₄₅Co₂₀Ni₁₅ high-entropy alloy. *J Alloy Compd* 809:151864. <https://doi.org/10.1016/j.jallcom.2019.151864>
- [123] Kim YK, Kim MC, Lee KA (2022) 1.45 GPa ultrastrong cryogenic strength with superior impact toughness in the in-situ nano oxide reinforced CrMnFeCoNi high-entropy alloy matrix nanocomposite manufactured by laser powder bed fusion. *J Mater Sci Technol* 97:10–19. <https://doi.org/10.1016/j.jmst.2021.04.030>
- [124] Curtze S, Kuokkala VT (2010) Dependence of tensile deformation behavior of TWIP steels on stacking fault energy, temperature and strain rate. *Acta Mater* 58:5129–5141. <https://doi.org/10.1016/j.actamat.2010.05.049>
- [125] Zhang R, Zhao S, Ding J, Chong Y, Jia T, Ophus C, Asta M, Ritchie RO, Minor AM (2020) Short-range order and its impact on the CrCoNi medium-entropy alloy. *Nature* 581:283–287. <https://doi.org/10.1038/s41586-020-2275-z>
- [126] Zhang YH, Zhuang Y, Hu A, Kai JJ, Liu CT (2017) The origin of negative stacking fault energies and nano-twin formation in face-centered cubic high entropy alloys. *Scr Mater* 130:96–99. <https://doi.org/10.1016/j.scriptamat.2016.11.014>
- [127] Wang M, Li Z, Raabe D (2018) In-situ SEM observation of phase transformation and twinning mechanisms in an interstitial high-entropy alloy. *Acta Mater* 147:236–246. <https://doi.org/10.1016/j.actamat.2018.01.036>
- [128] Ma L, Wang L, Nie Z, Wang F, Xue Y, Zhou J, Cao T, Wang Y, Ren Y (2017) Reversible deformation-induced martensitic transformation in Al_{0.6}CoCrFeNi high-entropy alloy investigated by in situ synchrotron-based high-energy X-ray diffraction. *Acta Mater* 128:12–21. <https://doi.org/10.1016/j.actamat.2017.02.014>
- [129] Shterner V, Timokhina IB, Beladi H (2016) On the work-hardening behaviour of a high manganese TWIP steel at different deformation temperatures. *Mater Sci Eng A* 669:437–446. <https://doi.org/10.1016/j.msea.2016.05.104>
- [130] Allain S, Chateau JP, Bouaziz O, Migot S, Guelton N (2004) Correlations between the calculated stacking fault energy and the plasticity mechanisms in Fe-Mn-C alloys. *Mater Sci Eng A* 387–389:158–162. <https://doi.org/10.1016/j.msea.2004.01.059>
- [131] Saeed-Akbari A, Mosecker L, Schwedt A, Bleck W (2011) Characterization and prediction of flow behavior in high-manganese twinning induced plasticity steels: part I. mechanism maps and work-hardening behavior. *Mater Trans A* 43:1688–1704. <https://doi.org/10.1007/s11661-011-0993-4>
- [132] Wang Z, Bei H, Baker I (2018) Microband induced plasticity and the temperature dependence of the mechanical properties of a carbon-doped FeNiMnAlCr high entropy alloy. *Mater Charact* 139:373–381. <https://doi.org/10.1016/j.matchar.2018.03.017>
- [133] Zhang X, Lin P, Huang JC (2020) Lattice distortion effect on incipient behavior of Ti-based multi-principal element alloys. *J Mater Res Technol* 9:8136–8147. <https://doi.org/10.1016/j.jmrt.2020.05.081>
- [134] Ding Q, Fu X, Chen D, Bei H, Gludovatz B, Li J, Zhang Z, George EP, Yu Q, Zhu T (2019) Real-time nanoscale observation of deformation mechanisms in CrCoNi-based medium- to high-entropy alloys at cryogenic temperatures. *Mater Today* 25:21–27. <https://doi.org/10.1016/j.mattod.2019.03.001>
- [135] Li W, Liu H, Yin P, Yan W, Wang W, Shan Y, Yang K (2022) Special tetrahedral twins in a cryogenically deformed CoCrFeNi high-entropy alloy. *J Mater Sci Technol* 100:129–136. <https://doi.org/10.1016/j.jmst.2021.05.045>
- [136] Tong Y, Chen D, Han B, Wang J, Feng R, Yang T, Zhao C, Zhao YL, Guo W, Shimizu Y, Liu CT, Liaw PK, Inoue K, Nagai Y, Hu A, Kai JJ (2019) Outstanding tensile properties of a precipitation-strengthened FeCoNiCrTi_{0.2} high-entropy alloy at room and cryogenic temperatures. *Acta Mater* 165:228–240. <https://doi.org/10.1016/j.actamat.2018.11.049>
- [137] Su J, Raabe D, Li Z (2019) Hierarchical microstructure design to tune the mechanical behavior of an interstitial TRIP-TWIP high-entropy alloy. *Acta Mater* 163:40–54. <https://doi.org/10.1016/j.actamat.2018.10.017>
- [138] Gutierrez-Urrutia I, Raabe D (2011) Dislocation and twin substructure evolution during strain hardening of an Fe-22wt.% Mn-0.6wt.% C TWIP steel observed by electron channeling contrast imaging. *Acta Mater* 59:6449–6462. <https://doi.org/10.1016/j.actamat.2011.07.009>
- [139] Fu Z, Chen W, Wen H, Zhang D, Chen Z, Zheng B, Zhou Y, Lavernia EJ (2016) Microstructure and strengthening mechanisms in an FCC structured single-phase nanocrystalline Co₂₅Ni₂₅Fe₂₅Al_{7.5}Cu_{17.5} high-entropy alloy. *Acta Mater* 107:59–71. <https://doi.org/10.1016/j.actamat.2016.01.050>
- [140] Li Z, Kormann F, Grabowski B, Neugebauer J, Raabe D (2017) Ab initio assisted design of quinary dual-phase high-entropy alloys with transformation-induced plasticity. *Acta Mater* 136:262–270. <https://doi.org/10.1016/j.actamat.2017.07.023>

- [141] Li ZM, Raabe D (2017) Strong and ductile non-equiautomic high-entropy alloys: design, processing, microstructure and mechanical properties. *JOM* 69:2099–2106
- [142] Li Z, Tasan CC, Pradeep KG, Raabe D (2017) A TRIP-assisted dual-phase high-entropy alloy: grain size and phase fraction effects on deformation behavior. *Acta Mater* 131:323–335. <https://doi.org/10.1016/j.actamat.2017.03.069>
- [143] Fang W, Chang R, Ji P, Zhang X, Liu B, Qu X, Yin F (2018) Transformation induced plasticity effects of a non-equal molar Co-Cr-Fe-Ni high entropy alloy system. *Metals* 8:369. <https://doi.org/10.3390/met8050369>
- [144] Jo YH, Choi WM, Sohn SS, Kim HS, Lee BJ, Lee S (2018) Role of brittle sigma phase in cryogenic-temperature-strength improvement of non-equi-atomic Fe-rich VCrMnFeCoNi high entropy alloys. *Mater Sci Eng A* 724:403–410. <https://doi.org/10.1016/j.msea.2018.03.115>
- [145] Lin QY, Liu JP, An XH, Wang H, Zhang Y, Liao XZ (2018) Cryogenic-deformation-induced phase transformation in an FeCoCrNi high-entropy alloy. *Mater Res Lett* 6(4):236–243. <https://doi.org/10.1080/21663831.2018.1434250>
- [146] Ma Y, Yang M, Yuan F, Wu X (2021) Deformation induced hcp nano-lamella and its size effect on the strengthening in a CoCrNi medium-entropy alloy. *J Mater Sci Technol* 82:122–134. <https://doi.org/10.1016/j.jmst.2020.12.017>
- [147] Sathiyamoorthi P, Moon J, Bae JW, Asghari-Rad P, Kim HS (2019) Superior cryogenic tensile properties of ultra-fine-grained CoCrNi medium-entropy alloy produced by high-pressure torsion and annealing. *Scr Mater* 163:152–156. <https://doi.org/10.1016/j.scriptamat.2019.01.016>
- [148] Tirunilai AS, Hanemann T, Reinhart C, Tschan V, Weiss KP, Laplanche G, Freudenberger J, Heilmair M, Kauffmann A (2020) Comparison of cryogenic deformation of the concentrated solid solutions CoCrFeMnNi, CoCrNi and CoNi. *Mater Sci Eng A* 783:139290. <https://doi.org/10.1016/j.msea.2020.139290>
- [149] Jo YH, Kim DG, Jo MC, Doh KY, Sohn SS, Lee D, Kim HS, Lee BJ, Lee S (2019) Effects of deformation-induced BCC martensitic transformation and twinning on impact toughness and dynamic tensile response in metastable VCrFeCoNi high-entropy alloy. *J Alloy Compd* 785:1056–1067. <https://doi.org/10.1016/j.jallcom.2019.01.293>
- [150] Song H, Kim DG, Kim DW, Jo MC, Jo YH, Kim W, Kim HS, Lee BJ, Lee S (2019) Effects of strain rate on room- and cryogenic-temperature compressive properties in metastable V₁₀Cr₁₀Fe₄₅Co₃₅ high-entropy alloy. *Sci Rep* 9:6163. <https://doi.org/10.1038/s41598-019-42704-x>
- [151] Pustovalov VV (2008) Serrated deformation of metals and alloys at low temperatures. *Low Temp Phys* 34(9):683. <https://doi.org/10.1063/1.2973710>
- [152] Wigley DA (1971) Mechanical properties of materials at low temperatures. Springer, New York. <https://doi.org/10.1007/978-1-4684-1887-3>
- [153] Moon J, Tabachnikova E, Shumilin S, Hryhorova T, Estrin Y, Brechtl J, Liaw PK, Wang W, Dahmen KA, Kim HS (2021) Unraveling the discontinuous plastic flow of a Co-Cr-Fe-Ni-Mo multiprincipal-element alloy at deep cryogenic temperatures. *Phys Rev Mater* 5:083601. <https://doi.org/10.1103/PhysRevMaterials.5.083601>
- [154] Wei D, Li X, Schönecker S, Jiang J, Choi WM, Lee BJ, Kim HS, Chiba A, Kato H (2019) Development of strong and ductile metastable face-centered cubic single-phase high-entropy alloys. *Acta Mater* 181:318–330. <https://doi.org/10.1016/j.actamat.2019.09.050>
- [155] Wei S, Kim J, Tasan CC (2019) Boundary micro-cracking in metastable Fe₄₅Mn₃₅Co₁₀Cr₁₀ high-entropy alloys. *Acta Mater* 168:76–78. <https://doi.org/10.1016/j.actamat.2019.01.036>

Publisher's Note Springer Nature remains neutral with regard to jurisdictional claims in published maps and institutional affiliations.